RESEARCH ARTICLE

Optimal timing of steroid initiation in response to CTLA-4 antibody in metastatic cancer: A mathematical model

Nourridine Siewe [1]*, **Avner Friedman** [2]

1 School of Mathematical Sciences, College of Science, Rochester Institute of Technology, Rochester, New York, United States of America, **2** Department of Mathematics, The Ohio State University, Columbus, Ohio, United States of America

* nourridine@aims.ac.za

Abstract

Immune checkpoint inhibitors, introduced in recent years, have revolutionized the treatment of many cancers. However, the toxicity associated with this therapy may cause severe adverse events. In the case of advanced lung cancer or metastatic melanoma, a significant number (10%) of patients treated with CTLA-4 inhibitor incur damage to the pituitary gland. In order to reduce the risk of hypophysitis and other severe adverse events, steroids may be combined with CTLA-4 inhibitor; they reduce toxicity, but they also diminish the anti-cancer effect of the immunotherapy. This trade-off between tumor reduction and the risk of severe adverse events poses the following question: What is the optimal time to initiate treatment with steroid. We address this question with a mathematical model from which we can also evaluate the comparative benefits of each schedule of steroid administration. In particular, we conclude that treatment with steroid should not begin too early, but also not very late, after immunotherapy began; more precisely, it should start as soon as tumor volume, under the effect of CTLA-4 inhibitor alone, begins to decrease. We can also compare the benefits of short term treatment of steroid at high doses to a longer term treatment with lower doses.

1 Introduction

Immune checkpoint inhibitors (ICI) is a type of immunotherapy that blocks membrane proteins, called checkpoints, on some T cells and cancer cells. It has revolutionized the treatment of various cancers, greatly prolonging the survival in advanced lung cancer, melanoma, and other cancers. However, severe side effects have emerged as a result of altering the natural immune response [1–3]. In particular, toxicity associated with ICI may result in pneumonitis, diarrhea, colitis, hepatitis, thyroid, and damage to the pituitary gland [1, 2, 4].

Steroids, or cortocosteroids, are anti-inflammatory drugs, frequently used in non-small cell lung cancer (NSCLC) and melanoma patients treated with ICI [5, 6]; they reduce toxicity, but also impair immunotherapy [7]. Steroids commonly used include prednisone and dexamethasone, that are known to decrease the number of cytotoxic lymphocytes [8, 9], hence also the concentration of inflammatory cytokines, such as IL-1, IL-6 and TNF-α [10]. Some studies

show that using steroid too early after infusion of ICI decreases progression free survival (PFS) and overall survival (OS) [5, 11–13], but a recent review on metastatic analysis suggests that steroids, that are used only to mitigate adverse events of ICI, do not negatively affect overall survival [14]. The question of timing steroid initiation and response rates to ICI in metastatic cancer was considered in recent review by Maslov et al. [13]. Patients whose treatment with steroid began less than 2 months from ICI infusion had shorter PFS and OS than those who began treatment after more than 2 months.

CTLA-4 blockade, by ipilimumab, introduced in recent years in the treatment of metastatic melanoma, NSCLC and other cancers, incurs severe adverse events associated with toxicity, as observed by the high levels of TNF-α [15]. One of the most common immune related adverse events (irAEs) is hypophysitis [16–18]. Hypophysitis is a chronic inflammatory disease of the pituitary gland [19]. Since regulation of the pituitary function is controlled by cytokines [20], increased levels of inflammatory cytokines may disrupt the function of the gland. Hypophysitis can occur as autoimmune disease (primary), or as side-effect of treatment with ICI (secondary) [2]. Histological assessment identified T cells and dendritic cells (DCs) among the inflammatory cells in the pituitary gland of patients with hypophysitis [19, 21–24]. Secondary hypophysitis occurs in significant number of patients receiving ICI [19, 22, 24]. A form of hypophysitis is observed in more than 10% of metastatic melanoma and NSCLC patients receiving ipilimumab [16, 17, 25]. The mechanism involved in the targeted CTLA-4 vs. PD-1/PD-L1 in cancer treatment are not well understood [26]. It has been shown that CTLA-4 is expressed in normal pituitary gland cells [21] which could possibly explain why pituitary dysfunction is the most common immune-response adverse event of patients receiving CTLA-4 inhibitor therapy and not patients receiving PD-1/PD-L1 inhibitor [26, 27].

In what follows we take hypophysitis to represent all the irAEs. Indeed, hypophysitis occurs in significant larger percentage (10%) than any other severe adverse event: Palmeonitis occurs in 1.4% of patients undergoing immunotherapy with ICI [28], pneumonitis in 2.7% [29], myocarditis in 1% [30], neurologic diseases, including nephropathy, in 2.9% [31], colitis in 5.7–9.1% [32], and sustained acute kidney injury in 8% of patients [33]. Pancreatitis is negligible [34], and liver toxicity and cirrhosis are not common [35].

In this paper we consider an hypothetical treatment group of patients with metastatic cancer for which simulations are made about treatment with ICI in combination with steroid given in a specific schedule, and use a mathematical model to evaluate the comparative benefits of each schedule of steroid administration by determining both cancer growth and the risk of irAEs. More precisely, we consider a patient with NSCLC or metastatic melanoma and compute, for specific schedules of administration of prednisone, the tumor volume profile and the risk of hypophysitis as determined by the level of toxicity. The primary inflammatory cytokines are IL-1, IL-6 and TNF-α, but, since IL-1 and IL-6 are produced primarily by macrophages [36, 37], we simplify the model by introducing only TNF-α (which is produced by inflammatory CD4$^+$ T cells [38]), and use the concentration of TNF-α to represent the level of toxicity. TNF-α diffuses from the tumor to the pituitary gland; an additional source of TNF-α originates in the pituitary gland as ipilimumab (which is infused into the blood) and targets the CTLA-4 expressed on pituitary cells. For simplicity, when considering levels of TNF-α below a prescribed threshold, we take the average concentration of TNF-α just within the tumor.

We develop a mathematical model based on the network in Fig 1. The model is represented by a system of partial differential equations, and is developed in a similar manner to other mathematical models of cancer-immune dynamics [39–46]. In [39], ICI was taken in combination with cancer vaccine, and, in [42], oncolytic virus therapy was supplemented by ICI; in [40], ICI was combined with BRAF/MEK inhibitor and in [41] it was combined with BET inhibitor, and combination of ICI with VEGF-inhibitor was considered in [43]. These papers
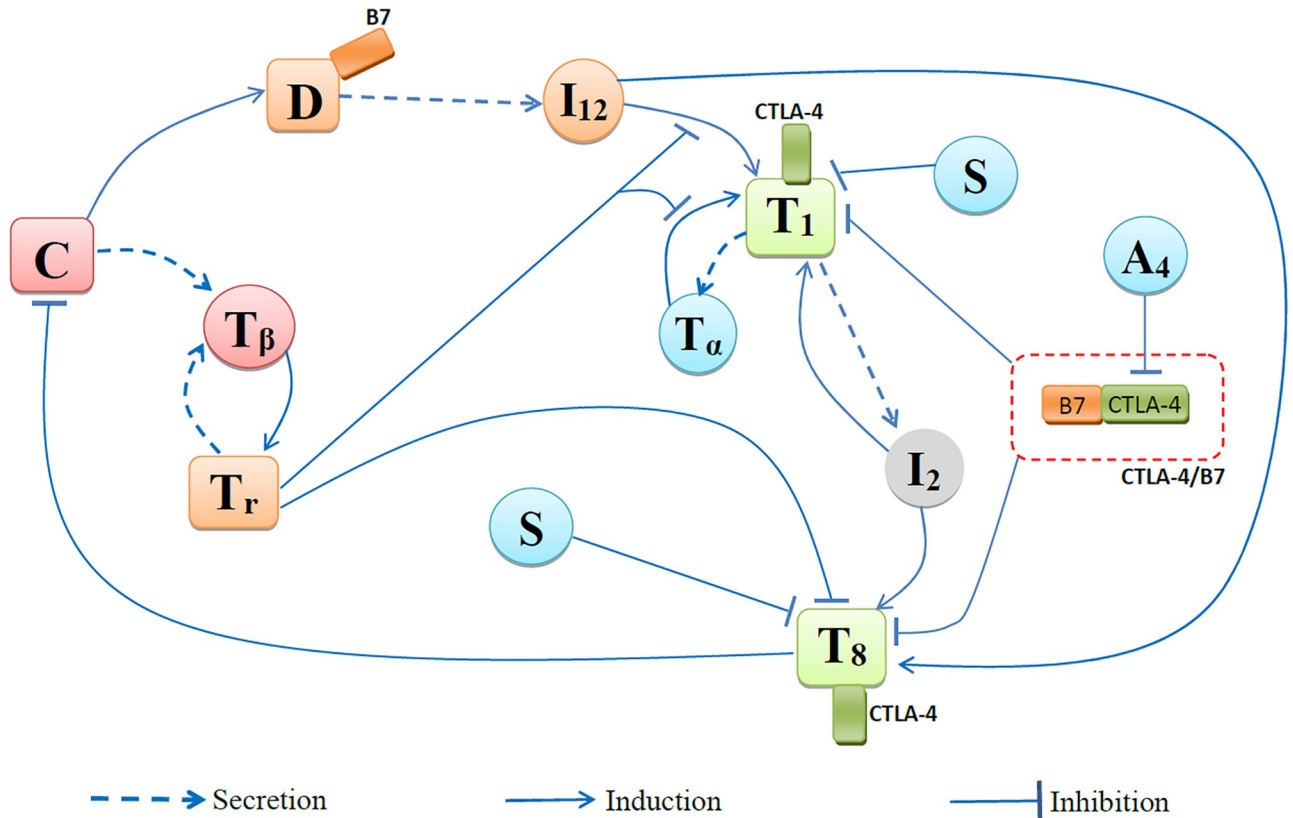
Fig 1. Network of cells and cytokines.

addressed the questions what are effective protocols in terms of the amount of dose of each agent and what are optimal schedules of administration of the drugs. Other articles addressed the issue of drug resistance. In [44], it was shown that ICI reduces resistance to hormone therapy in metastatic prostate cancer; in [45] it was shown that resistance to ICI is reduced by anti-TNF-α; and in [46] it was shown that primary resistance to ICI can be overcome by anti-TGF-β. There are several mathematical models that represent treatment of cancer by ICI in terms of ordinary differential equations. A combination of ICI with immunostimulant was modeled in [47] by a system of 4 ODEs, and the effect of PD-L1 on tumor was studied in [48] using ODEs in three interrelated compartments; tumor, blood and spleen. A combination of ICI therapy with radiation was considered in [49] by a PDE system, and in [50] by a system of finite differences.

The species in the network in Fig 1 include cancer cells (C), CD8$^+$ T cells (T_8), CD4$^+$ T cells (Th1 (T_1) and Tregs (T_r)), dendritic cells (D), and cytokines IL-2 (I_2), IL-12 (I_{12}), TGF-β (T_β) and TNF-α (T_α). The interactions among these species are represented by a system of partial differential equations (PDEs) in the tumor region $\Omega(t)$, which varies in time.

Dendritic cells (DCs), activated by cancer antigen, secrete IL-12, and IL-12 induces activation of naive CD4$^+$ T cells and naive CD8$^+$ T cells into T_1 and T_8 cells, respectively [51]. IL-2 is produced by T_1, and it induces proliferation of both T_1 and T_8 [52, 53]. Cancer cells are killed primarily by T_8 cells. The inflammatory TNF-α is produced by T_1 cells and it activates them [38]. TGF-β is secreted by cancer cells [54] and by T_r [55], it induces proliferation of T_r cells [56], and T_r blocks the activation of both T_1 and T_8 cells [55, 57].

Dendritic cells express ligand B7, and the complex B7/CTLA-4 blocks the activation of naive T cells into T_1 and T_8. Prednisone (S) reduces toxicity by depleting T_1 and T_8 cells.

The mathematical model is based on representing the dynamics of these interactions by a system of partial differential equations.

2 Mathematical model

Table 1 lists all the variables of the model in units of g/cm^3.

We denote the tumor region, at time t, by $\Omega(t)$. This region varies with time and so are the cells within it. We assume that all the cells, as well as the cytokines, move with the same velocity **u**, and that they are also undergoing dispersion (diffusion).

The variables X_i satisfy a system of partial differential equations of the form

$$\frac{\partial X_i}{\partial t} + \nabla \cdot (\mathbf{u}X_i) - \delta_{X_i}\nabla^2 X_i = F_i(X_1, \ldots, X_n) \text{ in } \Omega(t), \ (i = 1, \ldots, n), \tag{1}$$

where $F_i(X_1, \ldots, X_n)$ is determined from the network of Fig 1, and δ_{X_i} is the diffusion coefficient.

Equation for D

Immature dendritic cells (D_0) are activated by HMGB-1 produced by necrotic cancer cells [58–60]. We represent this activation by a Michaelis-Menten rate $\lambda_{DC}D_0 C/(K_C + C)$, where D_0 is the source of immature dendritic cells. Hence, the dynamics of DCs is given by

$$\frac{\partial D}{\partial t} + \nabla \cdot (\mathbf{u}D) - \delta_D \nabla^2 D = \lambda_{DC} D_0 \frac{C}{K_C + C} - \mu_D D, \tag{2}$$

where δ_D is the diffusion coefficient and μ_D is the death rate.

Equations for T_1 and T_8

Naive CD4$^+$ T cells, T_{10}, differentiate into T_1 cells under I_{12} [51] and T_α [38] environment, a process inhibited by T_r [55]. The proliferation of activated T_1 cells is enhanced by I_2 [52, 53]. Both processes of activation and proliferation are inhibited by the complex B7/CTLA-4 (Q), by a factor $1/(1 + Q/K_{TQ})$, and prednisone (S) depletes T_1 cells [8]. Hence, T_1 satisfies the

Table 1. Variables of the model. All densities and concentrations are in units of g/cm^3.

Variables	Descriptions		Variables	Descriptions
D	density of dendritic cells		T_1	density of Th1 cells
T_8	density of CD8$^+$ T cells		T_r	density of Treg cells
C	density of cancer cells			
I_2	concentration of IL-2		I_{12}	concentration of IL-12
T_α	concentration of TNF-α		T_β	concentration of TGF-β
B_7	concentration of B7		P_A	concentration of CTLA-4
Q	concentration of B7/CTLA-4			
A_4	concentration of anti-CTLA-4 (ipilimumab)		S	concentration of prednisone

following equation:

$$\frac{\partial T_1}{\partial t} + \nabla \cdot (\mathbf{u} T_1) - \delta_{T_1} \nabla^2 T_1 =$$

$$\left[T_{10} \left(\lambda_{T_1 I_{12}} \frac{I_{12}}{K_{I_{12}} + I_{12}} + \lambda_{T_1 T_\alpha} \frac{T_\alpha}{K_{T_\alpha} + T_\alpha} \right) \frac{1}{1 + T_r/K_{TT_r}} + \lambda_{T_1 I_2} T_1 \frac{I_2}{K_{I_2} + I_2} \right] \frac{1}{1 + Q/K_{TQ}} \quad (3)$$

$$- \mu_{T_1} T_1 - \mu_{ST} S T_1.$$

Similarly,

$$\frac{\partial T_8}{\partial t} + \nabla \cdot (\mathbf{u} T_8) - \delta_{T_8} \nabla^2 T_8 =$$

$$\left[T_{80} \left(\lambda_{T_8 I_{12}} \frac{I_{12}}{K_{I_{12}} + I_{12}} + \lambda_{T_8 T_\alpha} \frac{T_\alpha}{K_{T_\alpha} + T_\alpha} \right) \frac{1}{1 + T_r/K_{TT_r}} + \lambda_{T_8 I_2} T_8 \frac{I_2}{K_{I_2} + I_2} \right] \frac{1}{1 + Q/K_{TQ}} \quad (4)$$

$$- \mu_{T_8} T_8 - \mu_{ST} S T_8;$$

note that T_r also controls the activation of T_8 cells [57].

Equation for T_r

The activation of T_r is induced by TGF-β [56], so that

$$\frac{\partial T_r}{\partial t} + \nabla \cdot (\mathbf{u} T_r) - \delta_{T_r} \nabla^2 T_r = \lambda_{T_r T_\beta} T_{10} \frac{T_\beta}{K_{T_\beta} + T_\beta} - \mu_{T_r} T_r. \quad (5)$$

Equation for C

We assume logistic growth of cancer cells, with carrying capacity C_M, to account for their competition for space and nutrients. Cancer cells are killed primarily by CD8$^+$ T cells, hence

$$\frac{\partial C}{\partial t} + \nabla \cdot (\mathbf{u} C) - \delta_C \nabla^2 C = \lambda_C C \left(1 - \frac{C}{C_M} \right) - \mu_{T_8 C} T_8 C - \mu_C C, \quad (6)$$

where μ_C is the death rate of cancer cells, and $\mu_{T8}C$ is the rate by which T_8 cells kill cancer cells. As the network in Fig 1 shows, cancer cells try to block T_8 cells, but dendritic cells, activated by cancer antigen, lead to proliferation of T_8 cells; CTLA-4 inhibitor (A_4) increases the activation of T_8, and steroid (S) decreases it while reducing toxicity.

In order to determine the velocity $\mathbf{u}$, we need a constitutional assumption on the tumor tissue. For simplicity, we consider only the case of a spherically symmetric tumor and spherically symmetric variables. Then $\mathbf{u} = u \, \mathbf{e}_r$ where $\mathbf{e}_r$ is the unit radial vector, and $\Omega(t) = \{0 \leq r \leq R(t)\}$ is a sphere with boundary $r = R(t)$. In order to determine $u(r, t)$ we assume the combined density of all the cells in the tumor region $\Omega(t)$ remains constant in space and time, so that

$$D + T_1 + T_8 + T_r + C = \text{const.} \quad (7)$$

We then add all the cell equations and assume that their diffusion coefficients are approximately equal. Using Eq (7), we then obtain the following equation for $\mathbf{u}$:

$$\frac{1}{r^2} \frac{\partial}{\partial r} (r^2 u) = \nabla \cdot \mathbf{u} = \text{const} \cdot \Sigma \{\text{Right-hand-side of all cell equations}\}, \quad (8)$$

with $u(0, t) = 0$.

We assume that the boundary of $\Omega(t)$ varies with the velocity $\mathbf{u}$, hence

$$\frac{dR(t)}{dt} = u(R(t), t).$$

Equations for cytokines

IL-2 is produced by T_1 cells [52, 53], so that

$$\frac{\partial I_2}{\partial t} - \delta_{I_2} \nabla^2 I_2 = \lambda_{I_2 T_1} T_1 - \mu_{I_2} I_2, \tag{9}$$

where μ_{I_2} is a degradation rate. Note that the diffusion coefficient of cytokines is several orders of magnitude larger than the diffusion coefficient of cells, hence their advection velocity is negligible relative to their diffusion, and may therefore be dropped.

IL-12 is secreted by DCs [61, 62]. IL-12 is also secreted by iosinophils as a result of toxicity due to immunotherapy [63], which we assume to be proportional to A_4. Activated Th1 cells are the main receptors of IL-12, which means that they decrease IL-12 ligands in the process of being activated [64]. Hence,

$$\frac{\partial I_{12}}{\partial t} - \delta_{I_{12}} \nabla^2 I_{12} = \lambda_{I_{12} D} D + \lambda_{I_{12} A_4} A_4 - \mu_{I_{12} T_1} T_1 \frac{I_{12}}{K_{I_{12}} + I_{12}} - \mu_{I_{12}} I_{12}, \tag{10}$$

where $\mu_{I_{12}}$ is a degradation rate.

TNF-α is produced by T_1 cells [38], so that

$$\frac{\partial T_\alpha}{\partial t} - \delta_{T_\alpha} \nabla^2 T_\alpha = \lambda_{T_\alpha T_1} T_1 - \mu_{T_\alpha} T_\alpha. \tag{11}$$

TGF-β is produced by cancer cells [54] and T_r cells [55], hence

$$\frac{\partial T_\beta}{\partial t} - \delta_{T_\beta} \nabla^2 T_\beta = \lambda_{T_\beta C} C + \lambda_{T_\beta T_r} T_r - \mu_{T_\beta} T_\beta. \tag{12}$$

Equation for B7 (B_7), CTLA-4 (P_A) and B7/CTLA-4 (Q)

CTLA-4 is a receptor expressed on activated T_1 and T_8 cells [65] and the complex B7/CTLA-4 blocks the activities of these cells [65, 66]. CTLA-4 is constitutively expressed on T_r cells, but its activity is not blocked by the complex B7/CTLA-4 [67]. We assume that the number of CTLA-4 proteins per cell is the same for T_1 and T_8 cells, but different for T_r cells, by a factor κ_T. We denote by ρ_{P_A} the ratio between the mass of all CTLA-4 proteins in one T cell to the mass of this cell, so that

$$P_A = \rho_{P_A}(T_1 + T_8 + \kappa_T T_r).$$

The coefficient ρ_{P_A} is constant when no anti-CTLA-4 drug is administered. In this case, to a change in T (T_1, T_8, T_r), given by $\partial T / \partial t$, there corresponds a change of P_A, given by $\rho_{P_A} \partial T / \partial t$.

Similar changes in P_A arises from the terms of diffusion and advection, so that

$$
\frac{\partial P_A}{\partial t} + \nabla \cdot (\mathbf{u}P_A) - \delta_T \nabla^2 P_A =
$$

$$
\rho_{P_A} \Bigg\{ \left[\left((\lambda_{T_1 I_{12}} T_{10} + \lambda_{T_8 I_{12}} T_{80}) \frac{I_{12}}{K_{I_{12}} + I_{12}} + (\lambda_{T_1 T_\alpha} T_{10} + \lambda_{T_8 T_\alpha} T_{80}) \frac{T_\alpha}{K_{T_\alpha} + T_\alpha} \right) \frac{1}{1 + T_r/K_{TT_r}} \right.
$$

$$
\left. + (\lambda_{T_1 I_2} T_1 + \lambda_{T_8 I_2} T_8) \frac{I_2}{K_{I_2} + I_2} \right] \frac{1}{1 + Q/K_{TQ}}
$$

$$
+ \kappa_T \lambda_{T_r T_\beta} T_{10} \frac{T_\beta}{K_{T_\beta} + T_\beta} - (\mu_{T_1} T_1 + \mu_{T_8} T_8 + \mu_{ST} S(T_1 + T_8) + \kappa_T \mu_{T_r} T_r) \Bigg\}.
$$

When anti-CTLA-4 drug (A_4) is applied, CTLA-4 is depleted at a rate proportional to A_4, and, in this case, the ratio $P_A/(T_1 + T_8 + \kappa_T T_r)$ may change. In order to include in the model both cases, with and without anti-CTLA-4, we replace ρ_{P_A} in the above equation by $P_A/(T_1 + T_8 + \kappa_T T_r)$. Hence,

$$
\frac{\partial P_A}{\partial t} + \nabla \cdot (\mathbf{u}P_A) - \delta_T \nabla^2 P_A = \frac{P_A}{(T_1 + T_8 + \kappa_T T_r)}
$$

$$
\times \Bigg\{ \left[\left((\lambda_{T_1 I_{12}} T_{10} + \lambda_{T_8 I_{12}} T_{80}) \frac{I_{12}}{K_{I_{12}} + I_{12}} + (\lambda_{T_1 T_\alpha} T_{10} + \lambda_{T_8 T_\alpha} T_{80}) \frac{T_\alpha}{K_{T_\alpha} + T_\alpha} \right) \frac{1}{1 + T_r/K_{TT_r}} \right.
$$

$$
\left. + (\lambda_{T_1 I_2} T_1 + \lambda_{T_8 I_2} T_8) \frac{I_2}{K_{I_2} + I_2} \right] \frac{1}{1 + Q/K_{TQ}} \tag{13}
$$

$$
+ \kappa_T \lambda_{T_r T_\beta} T_{10} \frac{T_\beta}{K_{T_\beta} + T_\beta} - (\mu_{T_1} T_1 + \mu_{T_8} T_8 + \mu_{ST} S(T_1 + T_8) + \kappa_T \mu_{T_r} T_r) \Bigg\} - \mu_{P_A A_4} P_A A_4,
$$

where $\mu_{P_A A_4}$ is the depletion rate of CTLA-4 by anti-CTLA-4.

Ligand B7 is expressed on dendritic cells, so that

$$
B_7 = \rho_{B_7} D, \quad \rho_{B_7} = \text{constant}.
$$

B7 and CTLA-4 from the complex B7/CTLA-4 (Q) with association and disassociation rates $\alpha_{B_7 P_A}$ and μ_Q, respectively:

$$
B_7 + P_A \underset{\mu_Q}{\overset{\alpha_{B_7 P_A}}{\rightleftharpoons}} Q.
$$
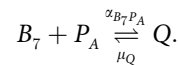
We assume that the half-life of Q is very short [68, 69], so that we may approximate the dynamics of Q by the steady state, $\alpha_{B_7 P_A} B_7 P_A = \mu_Q Q$, or

$$
Q = \sigma B_7 P_A, \tag{14}
$$

where $\sigma = \alpha_{B_7 P_A}/\mu_Q$.

Equations for A_4 and S

The concentration of anti-CTLA-4 satisfies the equation

$$
\frac{\partial A_4}{\partial t} - \delta_{A_4} \nabla^2 A_4 = \underbrace{\gamma_{A_4} f_{A_4}(t)}_{\text{source}} - \underbrace{\mu_{P_A A_4} P_A A_4}_{\text{depletion through blocking CTLA-4}} - \underbrace{\mu_{A_4} A_4}_{\text{degradation}} \tag{15}
$$

where the drug is injected at dose γ_{A_4} several times during treatment, and its actual strength at time t is $\gamma_{A_4}f_{A_4}(t)$.

Similarly, the concentration of prednisone satisfies the following equation:

$$\frac{\partial S}{\partial t} - \delta_S \nabla^2 S = \underbrace{\gamma_S f_S(t)}_{\text{source}} - \underbrace{\mu_{TS}(T_1 + T_8)S}_{\text{depletion through blocking } T_1 \text{ and } T_8} - \underbrace{\mu_S S}_{\text{degradation}} . \tag{16}$$

Boundary conditions

We assume that the tumor boundary, $\partial\Omega(t)$, is moving with velocity of the cells, that is

$$V_n = \mathbf{u} \cdot \mathbf{n} \tag{17}$$

where $\mathbf{n}$ is the outward normal at boundary and V_n is the velocity of the free boundary of the tumor in the direction $\mathbf{n}$.

We assume that the inactive CD4$^+$ and CD8$^+$ T cells that migrated from the lymph nodes into the tumor microenvironment have constant densities $\hat{T}_1$ and $\hat{T}_8$, respectively, at the tumor boundary, and that they are activated by IL-12 upon entering the tumor. We then have the following conditions at the tumor boundary:

$$\begin{aligned} \frac{\partial T_1}{\partial t} &+ \sigma_0 \frac{I_{12}}{K_{I_{12}} + I_{12}}(T_1 - \hat{T}_1)^+ = 0, \\ \frac{\partial T_8}{\partial r} &+ \sigma_0 \frac{I_{12}}{K_{I_{12}} + I_{12}}(T_8 - \hat{T}_8)^+ = 0 \quad \text{at } r = R(t). \end{aligned} \tag{18}$$

We impose no-flux boundary condition on all the remaining variables:

$$\text{No flux for } C, \ T_r, \ D, \ I_2, \ I_{12}, \ T_\alpha, \ T_\beta, \ P_A, \ A_4, \text{ and } S \text{ at } r = R(t); \tag{19}$$

it is tacitly assumed here that CTLA-4 become actives only after the T cells are already inside the tumor.

We prescribe initial conditions (in units of g/cm^3) after some time when the tumor was already established and the immune cells are activated:

$$\begin{aligned} C &= 0.41, \ T_1 = 10^{-3}, \ T_8 = 2.4 \times 10^{-4}, \ T_r = 10^{-5}, \ D = 10^{-6}, \\ I_2 &= 1.5 \times 10^{-11}, \ I_{12} = 5 \times 10^{-11}, \ T_\alpha = 4.4 \times 10^{-12}, \ T_\beta = 7.4 \times 10^{-9}, \text{ and } R = 0.13 \text{ cm.} \end{aligned} \tag{20}$$

Other nearby choices of initial conditions do not affect the simulations of the model after a few days.

3 Results

All the computations were done using Python 3.5.4. The parameter values of the model equations, except μ_{TS}, μ_{ST}, $\mu_{P_A A_4}$ and C_M, are estimated in Supporting Information and are listed in Tables 2 and 3. Parameter sensitivity analysis was performed using Latin Hypercube Sampling/Partial Rank Correlation Coefficient (LHS/PRCC) and presented in the Supporting Information, and the numerical scheme used in the simulations, the moving mesh method, is also described in the Supporting Information.

The simulations are carried out in the case of radially symmetric tumor, where $\Omega(t) = \{0 \leq r \leq R(t)\}$, and radially symmetric variables, that is, functions of (r, t), where $r = |x|$ is the distance of a point x to the origin, and $\mathbf{u} = u \, \mathbf{e}_r$ where $u = u(r, t)$ and $\mathbf{e}_r$ is the unit vector $x/|x|$.

Table 2. Parameters for the model.

Parameters	Descriptions	Values	references
λ_C	proliferation rate of C	0.203 d^{-1}	[75] est.
C_M	carrying capacity for N and M	4.9 g/cm^3	fitted
D_0	source of D	2×10^{-5} g/cm^3	[41]
T_{10}	source of T_1	4×10^{-4} g/cm^3	[41]
T_{80}	source of T_8	2×10^{-4} g/cm^3	[41]
$\hat{T}_1$	inflow of T_1 from lymph node	4×10^{-3} g/cm^3	[41]
$\hat{T}_8$	inflow of T_8 from lymph node	2×10^{-3} g/cm^3	[41]
μ_C	rate of death of C	0.17 d^{-1}	[76] est.
μ_D	rate of death of D	0.13 d^{-1}	[77] est.
μ_{T_1}	rate of death of T_1	0.2 d^{-1}	[78] est.
μ_{T_8}	rate of death of T_8	0.2 d^{-1}	[78] est.
μ_{T_r}	rate of death of T_r	0.25 d^{-1}	[79] est.
μ_{I_2}	rate of decay of I_2	166.22 d^{-1}	[80] est.
$\mu_{I_{12}}$	rate of decay of I_{12}	2.13 d^{-1}	[81] est.
μ_{T_α}	rate of decay of T_α	199 d^{-1}	[82, 83] est.
μ_{T_β}	rate of decay of T_β	399.25 d^{-1}	[46]
μ_{A_4}	decay rate of A_4	4.72×10^{-2} d^{-1}	[84] est.
μ_S	decay rate of S	4.62/5.54 d^{-1}	[73, 85] est.
μ_Q	decay rate of Q	6×10^4 d^{-1}	[68]
$\delta_C, \delta_D, \delta_T$	diffusion coefficient of cells	8.64×10^{-7} cm^{2}d^{-1}	[41] est.
δ_{I_2}	diffusion coefficient of I_2	9.92×10^{-2} cm^{2}d^{-1}	[86, 87] est.
$\delta_{I_{12}}$	diffusion coefficient of I_{12}	7.5×10^{-2} cm^{2}d^{-1}	[86, 87] est.
δ_{T_α}	diffusion coefficient of T_α	9.76×10^{-2} cm^{2}d^{-1}	[86, 88] est.
δ_{T_β}	diffusion coefficient of T_β	14.86×10^{-2} cm^{2}d^{-1}	[86, 89] est.
δ_{A_4}	diffusion coefficient of A_4	7.5×10^{-2} cm^{2}d^{-1}	[86, 90] est.
δ_S	diffusion coefficient of S	3.51×10^{-2} cm^{2}d^{-1}	[86, 91] est.
$\mu_{T_8 C}$	killing rate of C by T_8	33 cm^3/g·d	est.
$\mu_{P_A A_4}$	rate of depletion of A_4 by P_A	1.1×10^7 cm^3/g·d	fitted
μ_{ST}	inhibition rate of T_1 and T_8 by S	5.31×10^6 cm^3/g·d	fitted
μ_{TS}	absorption rate of S by T_1 and T_8	9×10^3 cm^3/g·d	fitted
$\mu_{I_{12} T_1}$	decay of I_{12} due to T_1 and T_8	10^{-7} cm^3/g·d	fitted

est.= this parameter was estimated in Supporting Information.

https://doi.org/10.1371/journal.pone.0277248.t002

Then Eq (17) becomes

$$\frac{dR(t)}{dt} = u(R(t), t). \tag{21}$$

From Eq (7) we then deduce that

$$\frac{dR(t)}{dt} = \frac{\theta}{R^2(t)} \int_0^{R(t)} \left[\sum_{j=2}^{6} \text{R.H.S. of Eqs. (2.j)} \right] r^2 dr. \tag{22}$$

Table 3. Parameters for the model (continued).

Parameters	Descriptions	Values	references
λ_{DC}	activation rate of D by C	$5.2 \ \mathrm{d}^{-1}$	est.
$\lambda_{T_1 I_2}$	proliferation rate of T_1 by I_2	$0.25 \ \mathrm{d}^{-1}$	[41]
$\lambda_{T_8 I_2}$	proliferation rate of T_8 by I_2	$0.25 \ \mathrm{d}^{-1}$	[41]
$\lambda_{T_1 I_{12}}$	activation rate of T_1 by I_{12}	$1.375 \ \mathrm{d}^{-1}$	est.
$\lambda_{T_8 I_{12}}$	activation rate of T_8 by I_{12}	$1.375 \ \mathrm{d}^{-1}$	est.
$\lambda_{T_1 T_\alpha}$	activation rate of T_1 by T_α	$4.125 \ \mathrm{d}^{-1}$	est.
$\lambda_{T_8 T_\alpha}$	activation rate of T_8 by T_α	$1.375 \ \mathrm{d}^{-1}$	est.
$\lambda_{T_r T_\beta}$	activation rate of T_r by T_β	$0.13 \ \mathrm{d}^{-1}$	est.
$\lambda_{I_2 T_1}$	production rate of I_2 by T_1	$1.6 \times 10^{-6} \ \mathrm{d}^{-1}$	est.
$\lambda_{I_{12} D}$	production rate of I_{12} by D	$3.03 \times 10^{-6} \ \mathrm{d}^{-1}$	est.
$\lambda_{I_{12} A_4}$	production rate of I_{12} due to A_4	$10^{-3} \ \mathrm{d}^{-1}$	est.
$\lambda_{T_\alpha T_1}$	production rate of T_α by T_1	$8.4 \times 10^{-7} \ \mathrm{d}^{-1}$	fitted
$\lambda_{T_\beta C}$	production rate of T_β by C	$7.2 \times 10^{-6} \ \mathrm{d}^{-1}$	est.
$\lambda_{T_\beta T_r}$	production rate of T_β by T_r	$3.6 \times 10^{-6} \ \mathrm{d}^{-1}$	est.
K_D	half saturation of D	$4 \times 10^{-4} \ \mathrm{g/cm^3}$	[41]
K_{TT_r}	inhibition of T_1 and T_8 by T_r	$1.04 \times 10^{-4} \ \mathrm{g/cm^3}$	[92] est.
K_{I_2}	half saturation of I_2	$1.9 \times 10^{-11} \ \mathrm{g/cm^3}$	[93] est.
$K_{I_{12}}$	half saturation of I_{12}	$10^{-10} \ \mathrm{g/cm^3}$	[93] est.
K_{T_α}	half saturation of T_α	$8.4 \times 10^{-12} \ \mathrm{g/cm^3}$	[88] est.
K_{T_β}	half saturation of T_β	$7.2 \times 10^{-9} \ \mathrm{g/cm^3}$	[46]
K_Q	half saturation of Q	$4.86 \times 10^{-20} \ \mathrm{g^2/cm^6}$	[41]
K'_{TQ}	inhibition of T_1 and T_8 by P_A-B_7	$4.86 \times 10^{-20} \ \mathrm{g^2/cm^6}$	[41]
θ	constant density of cells	$0.5 \ \mathrm{g/cm^3}$	est.
κ_T	($\#P_A$ per T_r)/($\#P_A$ per T_1 or T_8)	1	est.

est.= this parameter was estimated in Supporting Information.

Mice experiments

In order to determine the effect of steroid on the efficacy of ipilimumab, we use some data from mice experiments by Tokunaga et al. [70] and Giles et al. [9]. We assume that a drug A, with half-life m, injected at time $t = 0$ with dose A_0, degrades exponentially, so that

$$\frac{dA}{dt} = -A_0 e^{-\mu_A t},$$

where

$$\mu_A = \frac{\ln 2}{m}.$$

In the experiments in [70] Figs 1A, 1B and 3H (for convenience we have added this figure in the S1 Appendix), A_4 was injected in days 0, 3, 6 and S was injected in days 3, 5, 7 with low dose γ_S, and high dose $100\gamma_S$; the end-time was day 40. In the corresponding Eqs (15) and (16)

we then have,

$$f_{A_4}(t) = \begin{cases} e^{-\mu_{A_4}t}, & \text{for } 0 \le t < 3, \\ e^{-\mu_{A_4}t} + e^{-\mu_{A_4}(t-3)}, & \text{for } 3 \le t < 6, \\ e^{-\mu_{A_4}t} + e^{-\mu_{A_4}(t-3)} + e^{-\mu_{A_4}(t-6)}, & \text{for } t \ge 6, \end{cases}$$

$$f_S(t) = \begin{cases} e^{-\mu_S(t-3)}, & \text{for } 3 \le t < 5, \\ e^{-\mu_S(t-3)} + e^{-\mu_S(t-5)}, & \text{for } 5 \le t < 7, \\ e^{-\mu_S(t-3)} + e^{-\mu_S(t-5)} + e^{-\mu_S(t-7)}, & \text{for } t \ge 7. \end{cases}$$

The steroid used in [70] is methylprednisolone, which is slightly stronger than prednisone, but has a slightly shorter half-life.

Fig 2 shows the average densities/concentrations of all model's variables and the tumor volume during 40 days, A_4 as single agent, with A_4+low γ_S, and A_4+high γ_S, where $\gamma_{A_4} = 2 \times 10^{-8}$ g/cm^3·d, low $\gamma_S = 7 \times 10^{-9}$ g/cm^3·d, and high $\gamma_S = 700 \times 10^{-9}$ g/cm^3·d. Note that in the no-drug case, the slow increase in T_α is associated with the slow increase in T_1.

Fig 3 shows, more clearly, the profiles of tumor volume as they evolve from day to day. We see that, under treatment with A_4, the initial rate of increase of tumor volume begins to decrease around day 12 and to slowly change from increasing to decreasing, until it reaches the initial volume around day 40, where it shows tendency to slightly begin increasing.

Under A_4+low S, the volume profile is similar to that of the case of A_4, but the initial phases of increase and slowly changing to decrease end around day 32, and then the volume is continuously increasing. The volume profile under A_4+high S is similar, but the final increase occurs earlier, in day 28, and we see a significant increase by day 40 compared to the case of A_4+low
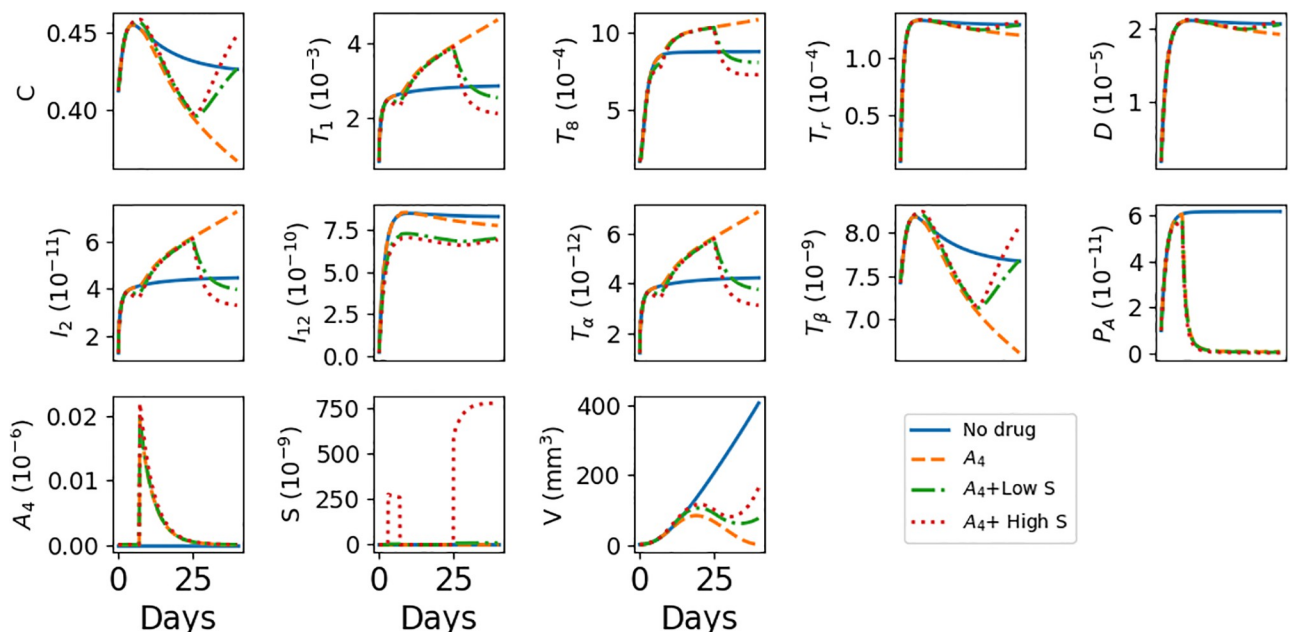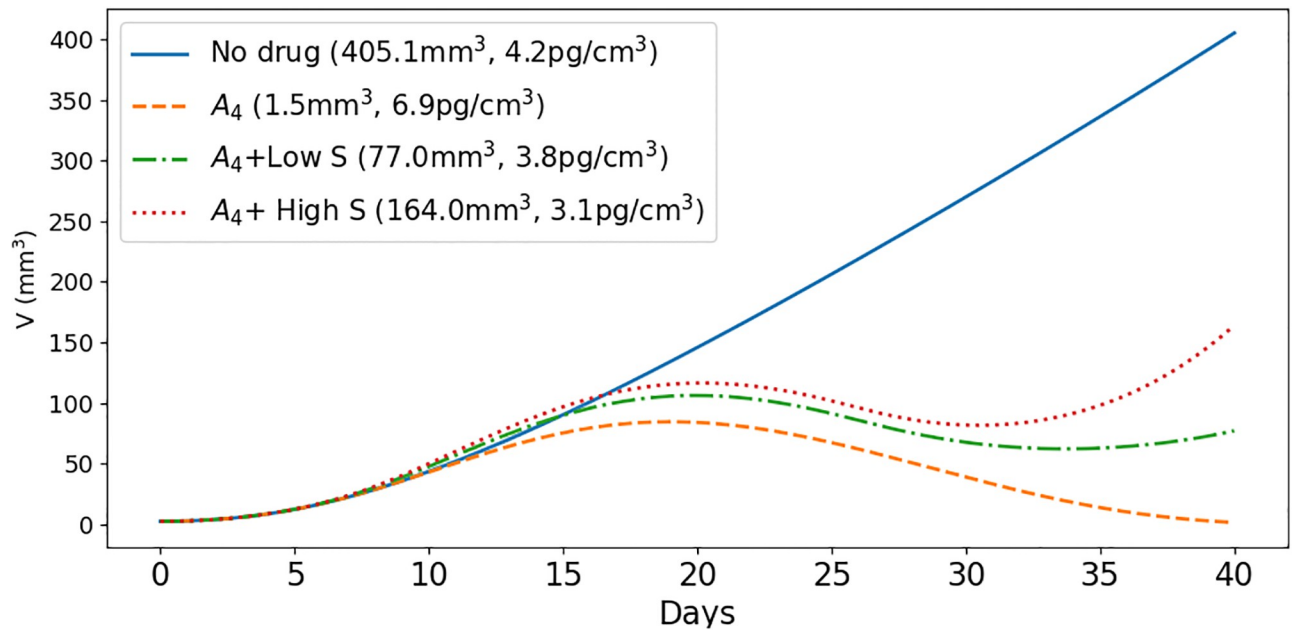

Fig 2. Simulation of the average densities/concentrations of the variables with/without anti-CTLA-4 and prednisone at $\gamma_{A_4} = 2 \times 10^{-8}$ g/cm^3·d, $\gamma_S = 7 \times 10^{-9}$ g/cm^3·d (low) and $\gamma_S = 700 \times 10^{-9}$ g/cm^3·d (high). All the model variables, with various drug combinations. All parameters are as in Tables 1 and 2 of Supplementary Information. A_4 alone reduces tumor growth but increases TNF-α, while A_4, when combined with S, reduces TNF-α but increases tumor growth. All species are in units of g/cm^3.

Fig 3. Simulation of the average densities/concentrations of the variables with/without anti-CTLA-4 and prednisone at $\gamma_{A_4} = 2 \times 10^{-8}$ g/cm^3·d, $\gamma_S = 7 \times 10^{-9}$ g/cm^3·d (low) and $\gamma_S = 700 \times 10^{-9}$ g/cm^3·d (high). Tumor volume only in various treatment combinations. All parameters are as in Tables 1 and 2 of Supplementary Information. A_4 alone reduces tumor growth but increases TNF-α, while A_4, when combined with S, reduces TNF-α but increases tumor growth. The pair (*, *) represents the tumor volume and the concentration of TNF-α at day 40. All species are in units of g/cm^3.

S. We also note that, under A_4+high S, tumor volume exceeds the control case during days 11–17.

All the above features are the same as in [70] Fig 1A and 1B, except that in [70] the changes from increase to decrease to increase occur earlier. This discrepancy may be explained by our choice of initial conditions which are not fitted to the actual experiment. We note that unlike methylprednisolone used in [70], prednisone, that will be used in our clinical trials, must first be converted in the liver into enzyme.

In Fig 4 we simulated the levels of IL-12 at day 40 in the cases of no-drug, A_4+low S, A_4+high S, and the maximum level attained by IL-12 in the course of treatment with A_4 alone, which occurs right after day 7 when the full dose of A_4 is given (note that in [70] Fig 3H the level of IL-12 was measured at day 10 right after the full dose of A_4 was given). We see that the level of IL-12 under A_4 is above the level of the control case (no drugs), and it decreases under A_4+low S to below the level of the control case; it further decreases under A_4+high S. This pattern is in agreement with [70] Fig 3H; although Fig 3H deals with the case of low affinity among CD8$^+$ T cells, this does not significantly affect dendritic cells and T_1 cells, and hence it also does not significantly affect IL-12 (by Eq (10)).

For the mice experiment settings [9], the tumor was treated with steroids from day 7 to the end-day, $t = 23$. So we may therefore take $f_S(t) = 0$ if $t < 7$ and $= 1$ if $t \geq 7$. A_4 was injected in days 13, 16 and 19. Fig 5 shows the level of T cells at the end-time under A_4 alone, S alone, and under the combination $A_4 + \gamma_S$. We see that under A_4, the IL-12 level is clearly above the control case, under $A_4 + \gamma_S$ it decreases below the control case, and the level under S alone is extremely small. This pattern is in agreement with [9] Fig 6a and 6b (for convenience we have added these figures in the S1 Appendix).
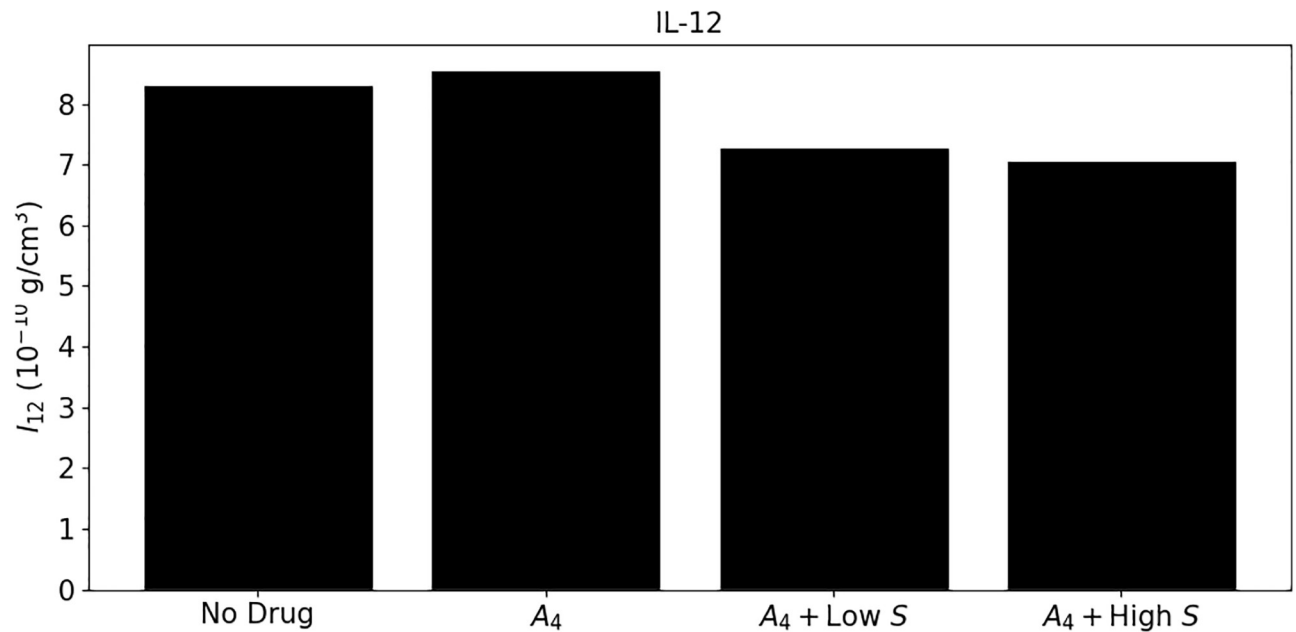
Fig 4. Levels of IL-12 with/without anti-CTLA-4 and prednisone at $\gamma_{A_4} = 2 \times 10^{-8}$ g/cm^3·d, $\gamma_S = 7 \times 10^{-9}$ g/cm^3·d (low) and $\gamma_S = 700 \times 10^{-9}$ g/cm^3·d (high).

https://doi.org/10.1371/journal.pone.0277248.g004

Clinical trials in silico

Having established qualitative agreement with some experimental results, we proceed to use the model in clinical trials framework, where treatments according to [71, 72] proceed in
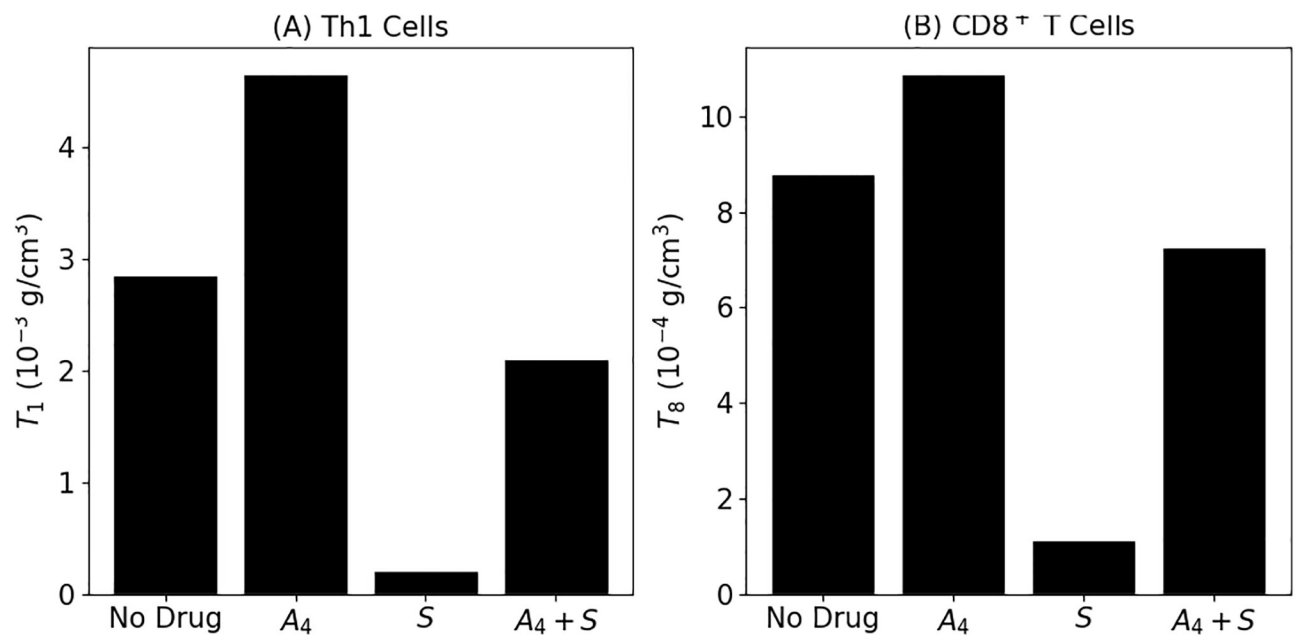

Fig 5. T cell levels with/without anti-CTLA-4 and prednisone at $\gamma_{A_4} = 2 \times 10^{-8}$ g/cm^3·d, $\gamma_S = 700 \times 10^{-9}$ g/cm^3·d (high) and $\gamma_S = 7000 \times 10^{-9}$ g/cm^3·d (alone). Density of Th1 cells (A) and density of CD8$^+$ T cells (B).

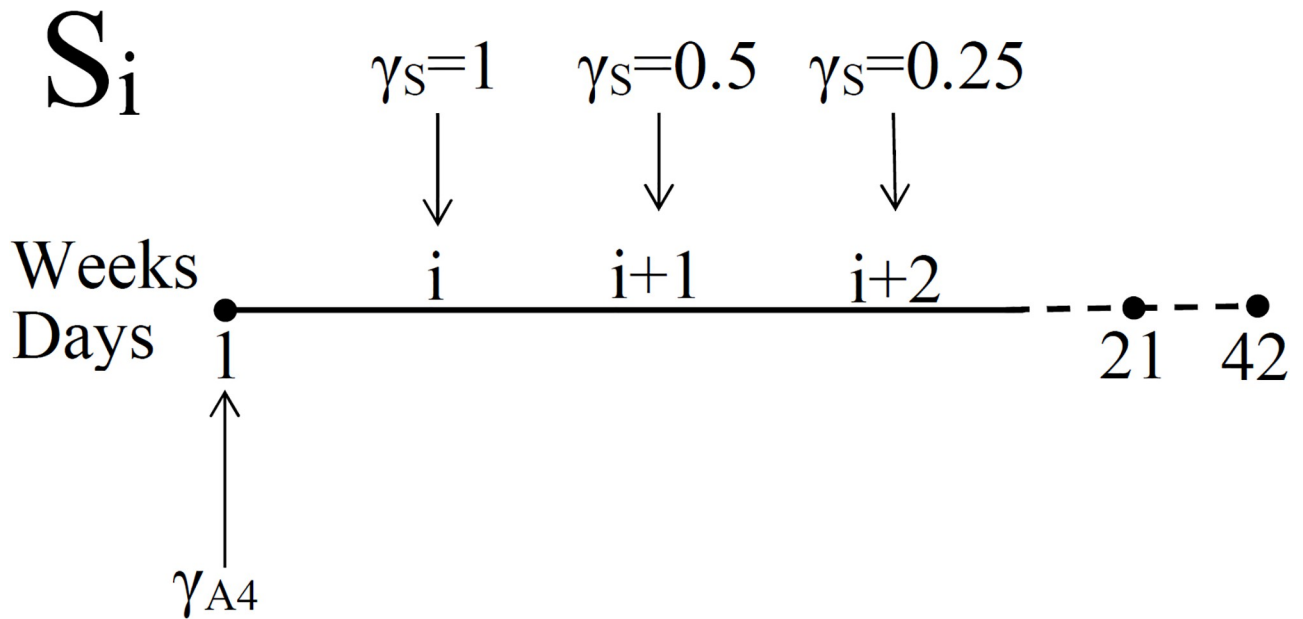https://doi.org/10.1371/journal.pone.0277248.g005

Fig 6. Schedules for administering steroid with doses γ_S = 1, 0.5 and 0.25 mg/kg·d. γ_{A_4} is a dose of anti-CTLA-4, is administered at days 1, 21 and 42.

https://doi.org/10.1371/journal.pone.0277248.g006

3-week cycles with ipilimumab administered (by infusion) on the first day of each of the first three cycles, at dose 3 mg/kg·d.

The average weight of people in the United States is 82 kg, which corresponds approximately to volume of 82×10^3 cm^3, this means that $\gamma_{A_4} = 3 \times 10^{-6}$ g/cm^3.

We shall simulate clinical trials seven cycles, so that

$$f_{A_4}(t) = \begin{cases} e^{-\mu_{A_4} t}, & \text{for } 0 \leq t < 21, \\ e^{-\mu_{A_4} t} + e^{-\mu_{A_4}(t-21)}, & \text{for } 21 \leq t < 42, \\ e^{-\mu_{A_4} t} + e^{-\mu_{A_4}(t-21)} + e^{-\mu_{A_4}(t-42)}, & \text{for } 42 \leq t \leq 63, \\ 0, & \text{for } t > 63 \end{cases}$$

where μ_{A_4} is the half-life of A_4.

The half-life of prednisone is 3–4 hours [73]; we take the average 3.5 hours, or equivalently, 0.15 days. Hence, μ_S = ln 2/0.15 = 4.62 d^{-1} and we may therefore assume that prednisone administered in one day has negligible level in the following days. On the other hand, since prednisone is usually taken in pills several times a day, we may take the level of the dose to remain constant during the day. Hence we define $f_S(t)$ in Eq (16) as follows:

$$f_S(t) = \begin{cases} 1, & \text{during the week that prednisone is administered,} \\ 0, & \text{otherwise.} \end{cases}$$

According to Aldea et al. [74], for non-severe irAEs, corticosteroid is given at daily amount 0.2 to 0.4 mg/kg for 2 to 3 weeks and then gradually tapered off during the following 2 to 4 weeks; but in the case of significant risk of severe irAEs, it is given in the same schedule in larger amount of 0.7 to 1 mg/kg per day.

We consider the following schedules for administering prednisone (represented schematically in Fig 6): Each treatment is 70 days long with

$$
\begin{aligned}
S_i: \quad \gamma_S &= 1 \ \mathrm{mg/kg \cdot d} \ \text{ in week } i \\
&= 0.5 \ \mathrm{mg/kg \cdot d} \ \text{ in week } i+1 \\
&= 0.25 \ \mathrm{mg/kg \cdot d} \ \text{ in week } i+2 \\
&= 0 \ \text{ in all other weeks}, \qquad \text{where } i = 1,\dots,7.
\end{aligned}
\tag{23}
$$

Note that 1 mg/kg·d, 0.5 mg/kg·d and 0.25 mg/kg·d correspond to 10^{-6}, 0.5×10^{-6} and 0.25×10^{-6} in g/cm³·d, respectively.

In what follows we use a simplified notation where $T_\alpha(t)$ denotes the average concentration of TNF-α in the tumor at time t, and $T_{\alpha,\mathrm{con}}(t)$ denotes $T_\alpha(t)$ in the control case (no drugs). Since hypophysitis does not occur in the control case, we assume that toxicity associated with this irAE is represented by the excess of $T_\alpha(t)$ over $T_{\alpha,\mathrm{con}}(t)$, and take the average of $[T_\alpha(t) - T_{\alpha,\mathrm{con}}(t)]^+$ over 70 days to represent the risk of hypophysitis; we denote this average by $T_{\alpha,\mathrm{ave}}(70)$, and denote the tumor volume at time t by $V(t)$.

Fig 7 left panel shows the profile of $T_\alpha(t)$ for each of the schedules S_i; the column indicates the corresponding volume $V(70)$, or $V(70; S_i)$. Fig 7 right panel shows the profile of $T_\alpha(t)$ for each schedule, and the column indicates the corresponding value of $T_{\alpha,\mathrm{ave}}(70)$, or $T_{\alpha,\mathrm{ave}}(70; S_i)$; $V(70, A_4)$ and $T_{\alpha,\mathrm{ave}}(70, A_4)$ correspond to the case when no steroids are given. We want to determine by the end of the first 3 cycles (day 70) in which anti-CTLA-4 is administered, when is the optimal time to start treatment with prednisone in order to keep toxicity as small as
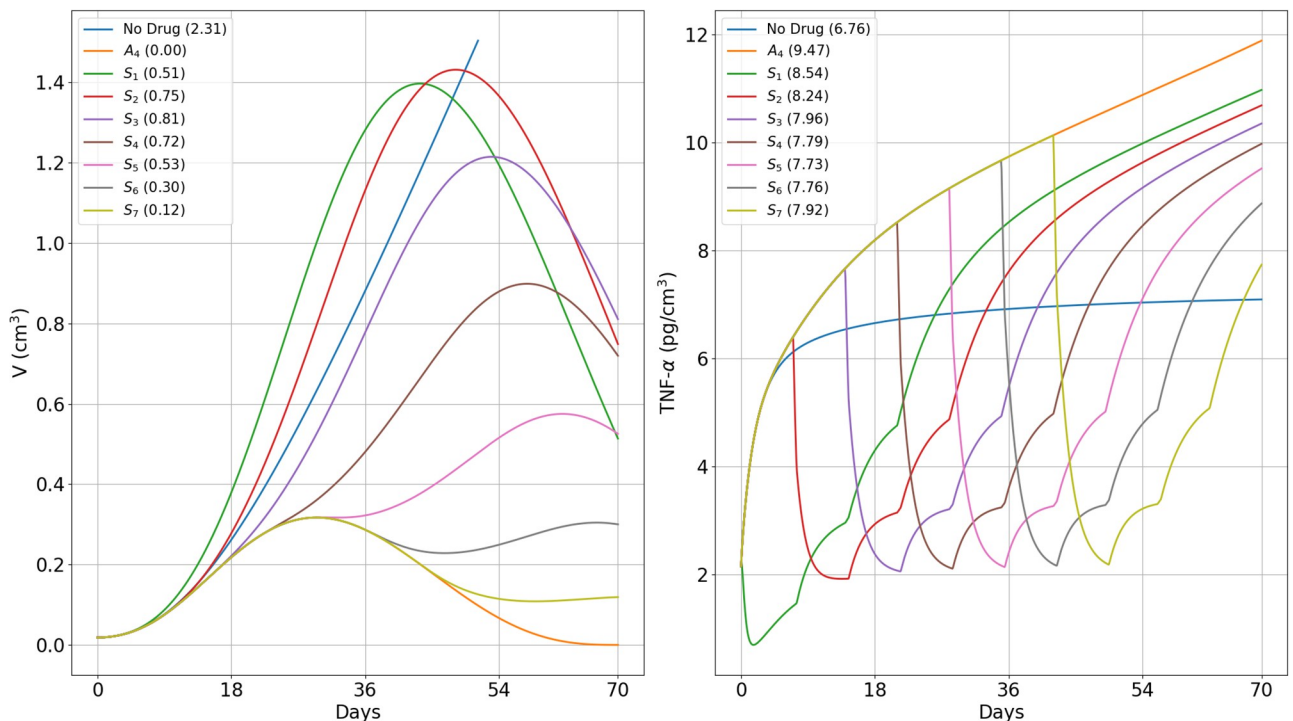

Fig 7. Different protocols of treatment with prednisone and anti-CTLA-4. $(S_1) - (S_7)$: Tumor volume (left) after 10 weeks and average TNF-α (right) A_4 is injected in the first day of each cycle, at $\gamma_{A_4} = 3 \times 10^{-6}$ g/cm³·d. S is given at various schedules (S_1)–(S_7) as in (23) at $\gamma_S = 10^{-6}$ g/cm³·d (1 mg/kg·d), $\gamma_S = 0.5 \times 10^{-6}$ g/cm³·d (0.5 mg/kg·d), and $\gamma_S = 0.25 \times 10^{-6}$ g/cm³·d (0.25 mg/kg·d). (a) The 10-week end-time tumor volumes are displayed on the left panels and the average of TNF-α taken over the levels that exceed the no-drug case, $T_{\alpha,\mathrm{ave}}$, on the right panel. Tumor volume at $t = 0$ is 0.01 cm³.

possible, while still decreasing tumor growth, and hopefully also keep volume as small as possible by the end-time of prednisone treatment, which we take to be day 126.

From Fig 7 we see that as i increases from 1 to 3, $V(70, S_i)$ increases and $T_{\alpha,\text{ave}}(70, S_i)$ decreases, and as i increases from 5 to 7, $V(70, S_i)$ decreases and $T_{\alpha,\text{ave}}(70, S_i)$ increases. So, there is a trade-off between tumor volume and associated toxicity. Interestingly, in the intermediate cases of $i = 4$ and $i = 5$,

$$V(70, S_5) < V(70, S_4) \quad \text{and} \quad T_{\alpha,\text{ave}}(70, S_5) < T_{\alpha,\text{ave}}(70, S_4),$$

which mean that schedule S_5 is better than schedule S_4.

Fig 7 right panel shows that $T_{\alpha,\text{ave}}(70, A_4) = 9.47$ pg/cm³. Although it is not possible to associate quantitatively the risk of hypophysis (which is 10% for patients of NSCLC and metastatic melanoma) for each S_i, it is clear that S_1 and S_2 schedules pose the largest risk (with $T_{\alpha,\text{ave}}(70)$) of above 8.24 pg/cm³, and even S_3 and S_7 have considerable risk. This means that steroid treatment should not start too early and not very late. The above comparison between S_4 and S_5 suggests that S_5 and possibly S_6, are the optimal schedules.

In Fig 8 we followed the growth of tumor volume after treatment, until day 126. We see that as i increases from 1 to 7, the volume $V(126, S_i)$ decreases as i increases. More specifically, $V(126, S_1) > 3V(126, S_2)$, $V(126, S_2) > 2V(126, S_3)$, $V(126, S_3)$ is nearly equal to $2V(126, S_4)$, and $V(126, S_4)$ is nearly equal to $2V(126, S_5)$. This says, even more strongly than Fig 7, that treatment with prednisone should not begin in the early weeks after treatment with ipilimumab had begun. The volumes $V(126, S_i)$ for $i = 5, 6, 7$, are very close to each other, but since S_7 incurs significant higher toxicity, options S_5 and S_6 still appear to the best.
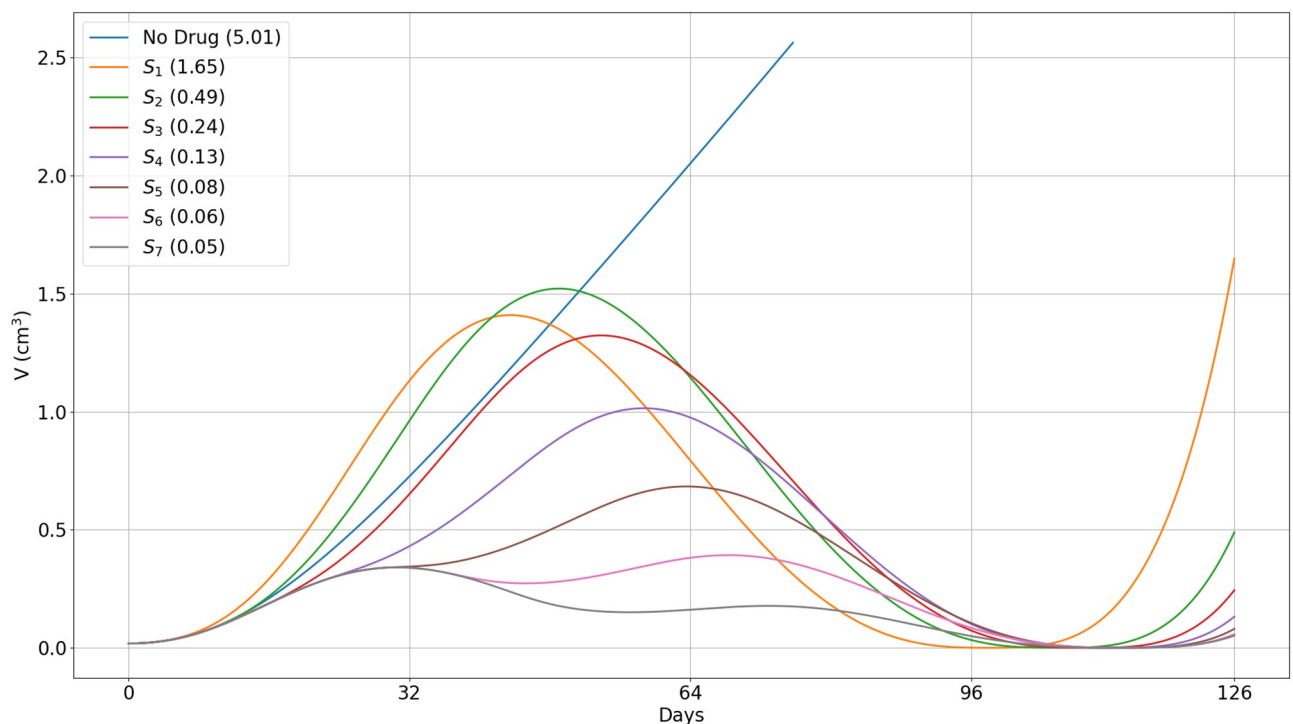

Fig 8. Different protocols of treatment with prednisone and anti-CTLA-4. (S_1) – (S_7): Tumor volume. A_4 is injected in the first day of each cycle, at $\gamma_{A_4} = 3 \times 10^{-6}$ g/cm³·d. S is given at various schedules (S_1)–(S_7) as in (23) at $\gamma_S = 10^{-6}$ g/cm³·d (1 mg/kg·d), $\gamma_S = 0.5 \times 10^{-6}$ g/cm³·d (0.5 mg/kg·d), and $\gamma_S = 0.25 \times 10^{-6}$ g/cm³·d (0.25 mg/kg·d). Tumor volume for 18 weeks. Tumor volume at $t = 0$ is 0.01 cm³.
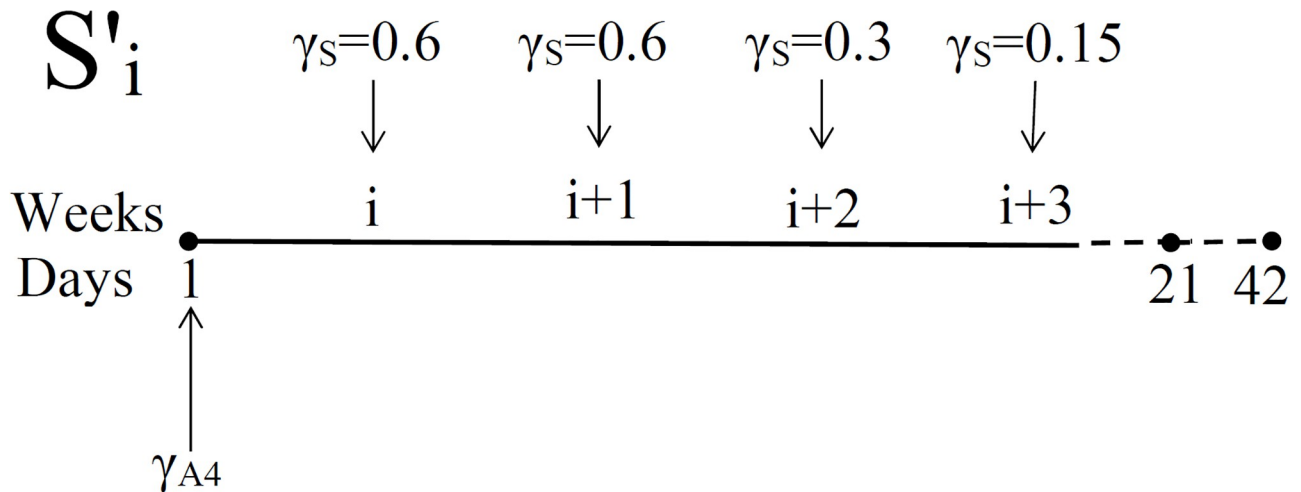
Fig 9. Schedules for administering steroid with doses γ_S = 0.6, 0.6, 0.3 and 0.15 mg/kg·d. γ_{A_4} is the dose of anti-CTLA-4, administered at days 1, 21 and 42.

https://doi.org/10.1371/journal.pone.0277248.g009

We may use the model to consider other protocols for prednisone administration. For example, the one shown in Fig 9, where

$$S'_i : \quad \gamma_S \quad = 0.6 \text{ mg/kg} \cdot \text{d in weeks } i \text{ and } i+1$$
$$= 0.3 \text{ mg/kg} \cdot \text{d in week } i+2$$
$$= 0.15 \text{ mg/kg} \cdot \text{d in week } i+3 \tag{24}$$
$$= 0 \text{ in the remaining weeks of the cycle}, \quad \text{where } i = 1, \ldots, 7.$$

Figs 10 and 11 show simulations similar to those in Figs 7 and 8, and we again conclude that treatment with prednisone should start not too early and not very late; as before, intermediate options S_5, and possibly S_6, are optimal.

4 Conclusion

Immune checkpoint inhibitors (ICI) have been introduced in recent years in the treatment of NSCLC and metastatic melanoma. However, by inhibiting negative regulation of inflammatory T cells, this treatment elicits toxicity which results in severe adverse events, including damage to organs such as the pituitary gland, where 10% of patients receiving CTLA-4 inhibitor (ipilimumab) develop hypophysitis. Steroids are known to decrease the number of inflammatory T cells and may therefore be used with ICI in order to reduce the risk of adverse events. But steroids also have the effect of increasing the tumor. The opposite effects of steroid on patient's health raises the following question: What is the optimal time for steroid initiation. This question was considered in several studies. Meta-analysis of such studies shows that patients whose treatment with steroid began less than 2 months from ICI initiation had shorter OS than those who began treatment after 2 months [13].

In this paper we consider patients of NSCLC or metastatic melanoma who are treated with CTLA-4 inhibitor (ipilimumab), and thus are at risk of severe adverse events, such as permanent damage to a vital organ. We take the pituitary gland to represent these organs, since hypophysitis occurs at significantly larger percentage than other damaged organs.

We assume that the risk of hypophysitis is the result of toxicity due to treatment with CTLA-4 inhibitor, and we represent the level of toxicity by the concentration of TNF-α in the
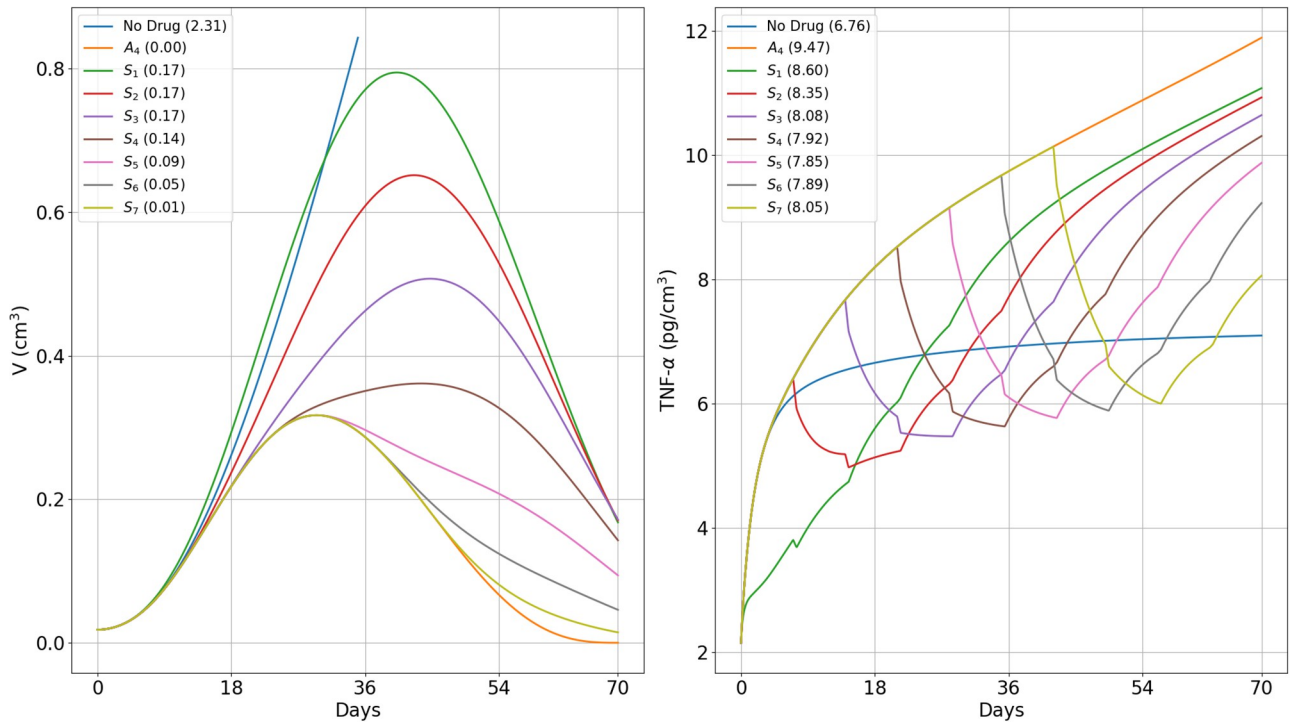
Fig 10. Different protocols of treatment with prednisone and anti-CTLA-4. $(S_1') - (S_7')$: Tumor volume (left) after 10 weeks and average TNF-α (right). A_4 is injected in the first day of each cycle, at $\gamma_{A_4} = 3 \times 10^{-6}$ g/cm^3·d. S is given at various schedules (S_1')–(S_7') as in (23) at $\gamma_S = 0.6 \times 10^{-6}$ g/cm^3·d (0.6 mg/kg·d), $\gamma_S = 0.3 \times 10^{-6}$ g/cm^3·d (0.3 mg/kg·d), and $\gamma_S = 0.15 \times 10^{-6}$ g/cm^3·d (0.15 mg/kg·d). The 10-week end-time tumor volumes are displayed on the left panels and the average of TNF-α taken over the levels that exceed the no-drug case, $T_{\alpha,\text{ave}}$, on the right panel. Tumor volume at $t = 0$ is 0.01 cm^3.

https://doi.org/10.1371/journal.pone.0277248.g010

tumor. We developed a mathematical model in order to determine optimal scheduling of treatment with steroid. The model is represented by a dynamical system of partial differential equations with variables that include cancer cells, immune cells, cytokines, and the two drug drugs (ipilimumab and prednisone). Most of the equations, as well as the estimates of the parameters and their sensitivity analysis, are given in Supplement Information; we have shown that the model simulations agree with mice experiments in [9, 74].

We then proceeded to simulate clinical trials in three 3-week cycles: Ipilimumab is infused at the beginning of each of the first three cycles, and steroid, with schedule S_i, begins at week i, for 3 or 4 weeks duration, where a large dose given in the early week(s) is tapered off during the remaining weeks. We took $i = 1, 2, \ldots, 7$, and treatment was evaluated at day 70.

We simulated the outcome of each schedule up to day 126, and computed two quantities:

$$T_{\alpha,\text{ave}}(70, S_i) \quad = \text{Average of } T_\alpha - T_{\alpha,\text{con}} \text{ at day 70,}$$
$$V(70, S_i), V(126, S_i) \quad = \text{Volume of tumor at days 70, 126,}$$

where $T_{\alpha,\text{con}}$ is the average concentration of TNF-α in the control case (no drugs) when we know that hypophysitis does not occur; $T_{\alpha,\text{con}}(t)$ is approximately 6.76 pg/cm^3. In the case when no steroid is given, $T_{\alpha,\text{ave}}(70) = 9.47$ pg/cm^3, and this level of toxicity corresponds to 10% risk of hypophysitis. This gives us some idea about the risk of hypophysitis in terms of the level of $T_{\alpha,\text{ave}}(70, S_i)$.

The values of the pairs $(T_\alpha(70, S_i), V(70, S_i))$ can be used to compare the benefits of each schedule of steroid administration and the optimal schedules were supported by the values of
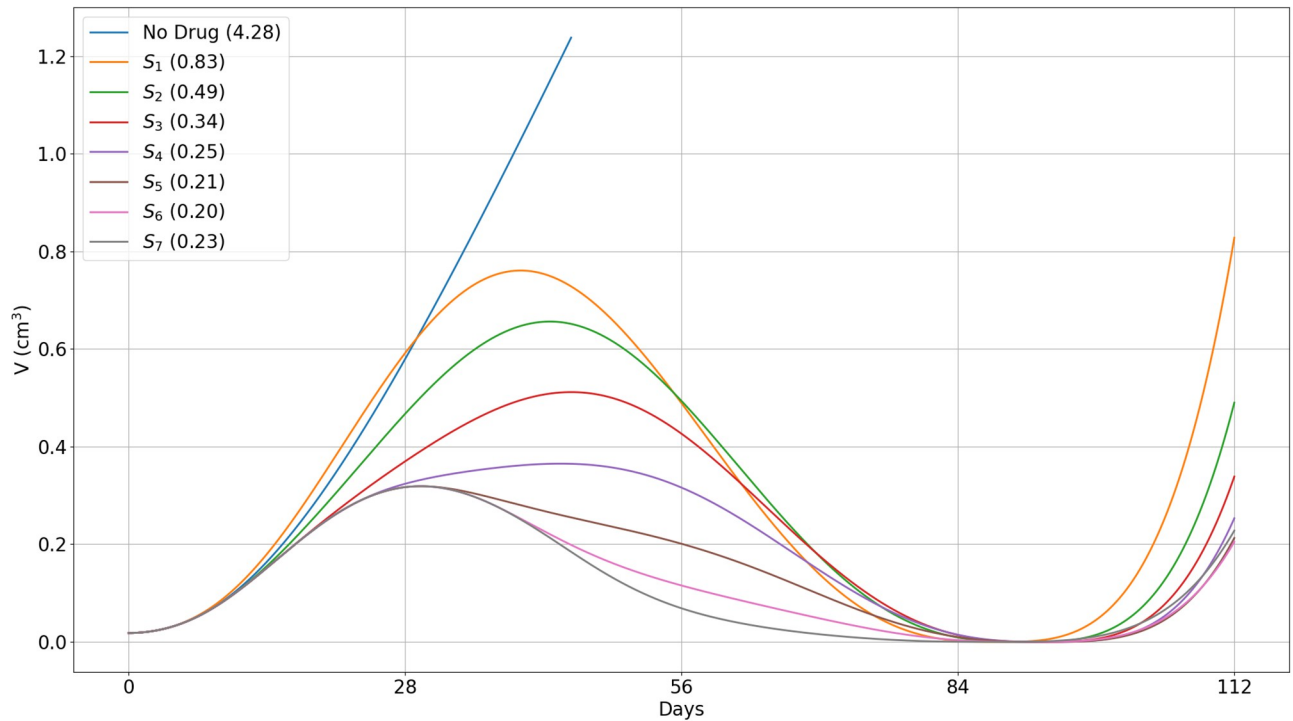
Fig 11. Different protocols of treatment with prednisone and anti-CTLA-4. $(S'_1) - (S'_7)$: Tumor volume. A_4 is injected in the first day of each cycle, at $\gamma_{A_4} = 3 \times 10^{-6}$ g/cm³·d. S is given at various schedules (S'_1)–(S'_7) as in (23) at $\gamma_S = 0.6 \times 10^{-6}$ g/cm³·d (0.6 mg/kg·d), $\gamma_S = 0.3 \times 10^{-6}$ g/cm³·d (0.3 mg/kg·d), and $\gamma_S = 0.15 \times 10^{-6}$ g/cm³·d (0.15 mg/kg·d). Tumor volume for 16 weeks. Tumor volume at $t = 0$ is 0.01 cm³.

https://doi.org/10.1371/journal.pone.0277248.g011

$V(126, S_i)$. In particular, we conclude that treatment with prednisone should not start in the first 4 weeks (too early) and not in week 7 (very late); schedules S_5, and possibly S_6, are the optimal ones; more generally, treatment with prednisone should start as soon as tumor volume, under the effect of CTLA-4 inhibitor alone, begins to decrease. We can also use the same pairs to compare the benefits of short time administration of steroid at total high dose with longer time administration at lower doses. For example, in, 3-week treatment with doses of 1, 0.5 and 0.25 mg/kg·d, we get, by Figs 7 and 8,

$$T_\alpha(70, S_5) = 7.73 \text{ pg/cm}^3, \quad V(70, S_5) = 0.53 \text{ cm}^3, \quad V(126, S_5) = 0.08 \text{ cm}^3,$$

while in, 4-week treatment with 0.6, 0.6, 0.3 and 0.15 mg/kg·d, we get, by Figs 10 and 11,

$$T_\alpha(70, S'_5) = 7.85 \text{ pg/cm}^3, \quad V(70, S'_5) = 0.09 \text{ cm}^3, \quad V(112, S'_5) = 0.21 \text{ cm}^3,$$

i.e., slightly more toxicity and larger cancer volume than in the 3-week treatment (already by day 112) with higher doses. Hence the particular 3-week schedule of steroid treatment is better than the 4-week schedule.

The paper has several limitations:

1. The conclusion arrived at on optimal scheduling of prednisone were based on short term evaluation. In order to gain more confidence in such conclusions, long term evaluations will be needed whereby anti-CTLA-4 is administered for larger number of cycles, and assessment is done at some times during treatment and, longer times, after the end of treatment.

2. The strategy for administering prednisone used in this paper is to start with a high dose, and continue decreasing the level of doses in the following weeks. But many other strategies could be considered, for example, intermittent treatment with high/medium dose of prednisone on weeks 2, 4 and 6, or 3, 5 and 6.

3. Toxicity was represented only by TNF-α that is produced by T_1 cells; IL-1 and IL-6 were omitted since they are secreted primarily by macrophages [36, 37] and, hence, are not appreciably affected by CTLA-4 inhibitor. If we were to include macrophages with its associated cytokines, the model's complexity will be significantly increased and so will the level of inaccuracies in estimating parameters.

4. The mechanism that leads from toxicity to hypophysitis was not considered, and the level of toxicity, by TNF-α, was taken only within the tumor.

5. Clinical studies shows that 10% of NSCLC and metastatic melanoma patients treated with CTLA-4 inhibitor develop hypophysitis, and our model shows that the corresponding level of TNF-α about the control level ($T_{\alpha,\text{ave}}(70)$) is 9.47 pg/ml. However, we are unable to fit a lower threshold of TNF-α with exact percentage of patients that will develop hypophysitis.

6. The level of TNF-α in homeostasis varies among people, and the average level among various studies varies greatly.

Nevertheless, the mathematical model provides a conceptual framework for assessing options of administering steroids with ICI, and could serve a useful prognostic tool in designing clinical trials with CTLA-4 inhibitor in combination with PD-1 or PD-L1 inhibitor, and chemotherapeutic drugs.

Supporting information

S1 File. Model equations, Parameters estimates, sensitivity analysis, numerical methods and tables of parameters.
(PDF)

S1 Appendix.
(PDF)

Author Contributions

Conceptualization: Nourridine Siewe, Avner Friedman.

Data curation: Nourridine Siewe, Avner Friedman.

Formal analysis: Nourridine Siewe, Avner Friedman.

Funding acquisition: Nourridine Siewe, Avner Friedman.

Investigation: Nourridine Siewe, Avner Friedman.

Methodology: Nourridine Siewe, Avner Friedman.

Project administration: Nourridine Siewe, Avner Friedman.

Resources: Nourridine Siewe, Avner Friedman.

Software: Nourridine Siewe.

Validation: Nourridine Siewe, Avner Friedman.

Visualization: Nourridine Siewe, Avner Friedman.

Writing – original draft: Nourridine Siewe, Avner Friedman.

Writing – review & editing: Nourridine Siewe, Avner Friedman.

References

1. Wang DY, Johnson DB, Davis EJ. Toxicities Associated With PD-1/PD-L1 Blockade. Cancer J. 2018; 24(1):36–40. https://doi.org/10.1097/PPO.0000000000000296 PMID: 29360726

2. Winer A, Bodor JN, Borghaei H. Identifying and managing the adverse effects of immune checkpoint blockade. J Thorac Dis. 2018; 10(Suppl 3):S480–S489. https://doi.org/10.21037/jtd.2018.01.111 PMID: 29593893

3. Scarpati GDV, Fusciello C, Perri F, Sabbatino F, Ferrone S, Carlomagno C, et al. Ipilimumab in the treatment of metastatic melanoma: management of adverse events. OncoTargets and therapy. 2014; 7:203–209. https://doi.org/10.2147/OTT.S57335

4. Kichloo A, Albosta M, Dahiya D, Guidi JC, Aljadah M, Singh J, et al. Systemic adverse effects and toxicities associated with immunotherapy: A review. World J Clin Oncol. 2021; 12(3):150–163. https://doi.org/10.5306/wjco.v12.i3.150 PMID: 33767971

5. Fucà G, Galli G, Poggi M, Lo Russo G, Proto C, Imbimbo M, et al. Modulation of peripheral blood immune cells by early use of steroids and its association with clinical outcomes in patients with metastatic non-small cell lung cancer treated with immune checkpoint inhibitors. ESMO Open. 2019; 4(1): e000457. https://doi.org/10.1136/esmoopen-2018-000457 PMID: 30964126

6. So ACP, Board RE. Real-world experience with pembrolizumab toxicities in advanced melanoma patients: a single-center experience in the UK. Melanoma Manag. 2018; 5(1). https://doi.org/10.2217/mmt-2017-0028 PMID: 30190931

7. Della Corte CM, Morgillo F. Early use of steroids affects immune cells and impairs immunotherapy efficacy. ESMO Open. 2019; 4(1):e000477. https://doi.org/10.1136/esmoopen-2018-000477 PMID: 30964127

8. Schuyler MR, Gerblich A, Urda G. Prednisone and T-Cell Subpopulations. Arch Intern Med. 1984; 144(5):973–975. https://doi.org/10.1001/archinte.1984.00350170119021 PMID: 6231898

9. Giles AJ, Hutchinson MND, Sonnemann HM, Jung J, Fecci PE, Ratnam NM, et al. Dexamethasone-induced immunosuppression: mechanisms and implications for immunotherapy. J Immunother Cancer. 2018; 6(1):51. https://doi.org/10.1186/s40425-018-0371-5 PMID: 29891009

10. O'Connor TM, O'Halloran DJ, Shanahan F. The stress response and the hypothalamic-pituitary-adrenal axis: from molecule to melancholia. QJM. 2020; 93(6):323–333. https://doi.org/10.1093/qjmed/93.6.323

11. De Giglio A, Mezquita L, Auclin E, Blanc-Durand F, Riudavets M, Caramella C, et al. Impact of Intercurrent Introduction of Steroids on Clinical Outcomes in Advanced Non-Small-Cell Lung Cancer (NSCLC) Patients under Immune-Checkpoint Inhibitors (ICI). Cancers (Basel). 2020; 12(10):2827. https://doi.org/10.3390/cancers12102827

12. Arbour KC, Mezquita L, Long N, Rizvi H, Auclin E, Ni A, et al. Impact of Baseline Steroids on Efficacy of Programmed Cell Death-1 and Programmed Death-Ligand 1 Blockade in Patients With Non-Small-Cell Lung. Cancer J Clin Oncol. 2018; 36(28):2872–2878. PMID: 30125216

13. Maslov DV, Tawagi K, Madhav KC, Simenson V, Yuan H, Parent C, et al. Timing of steroid initiation and response rates to immune checkpoint inhibitors in metastatic cancer. J ImmunoTher Cancer. 2021; 9(e002261). https://doi.org/10.1136/jitc-2020-002261 PMID: 34226279

14. Petrelli F, Signorelli D, Ghidini M, Ghidini A, Pizzutilo EG, Ruggieri L, et al. Association of Steroids use with Survival in Patients Treated with Immune Checkpoint Inhibitors: A Systematic Review and Meta-Analysis. Cancers. 2020; 12(3):546. https://doi.org/10.3390/cancers12030546 PMID: 32120803

15. Laurent S, Queirolo P, Boero S, Salvi S, Piccioli P, Boccardo S, et al. The engagement of CTLA-4 on primary melanoma cell lines induces antibody-dependent cellular cytotoxicity and TNF-α production. J Transl Med. 2013; 11(108). https://doi.org/10.1186/1479-5876-11-108 PMID: 23634660

16. Tsoli M, Kaltsas G, Angelousi A, Alexandraki K, Randeva H, Kassi E. Managing Ipilimumab-Induced Hypophysitis: Challenges and Current Therapeutic Strategies. Cancer Manag Res. 2020; 12:9551–9561. https://doi.org/10.2147/CMAR.S224791 PMID: 33061641

17. Wei KZ, Baxter M, Casasola R. Hypophysitis induced by immune checkpoint inhibitors in a Scottish melanoma population. Melanoma Manag. 2019; 6(1). https://doi.org/10.2217/mmt-2018-0009 PMID: 31236205

18. Castillero F, Castillo-Fernández O, Jiménez-Jiménez G, Fallas-Ramírez J, Peralta-Alvarez MP, Arrieta O. Cancer immunotherapy-associated hypophysitis. Future Oncol. 2019; 15(27):3159–3169. https://doi.org/10.2217/fon-2019-0101 PMID: 31423850

19. Kluczyński L, Gilis-Januszewska A, Rogoziński D, Pantofliński J, Hubalewska-Dydejczyk A. Hypophysitis—new insights into diagnosis and treatment. Endokrynol Pol. 2019; 70(3):260–269. https://doi.org/10.5603/EP.a2019.0015 PMID: 31290557

20. Haedo MR, Gerez J, Fuertes M, Giacomini D, Páez-Pereda M, Labeur M, et al. Regulation of pituitary function by cytokines. Horm Res. 2009; 72(5):266–274. PMID: 19844112

21. Caturegli P, Di Dalmazi G, Lombardi M, Grosso F, Larman HB, Larman T, et al. Hypophysitis Secondary to Cytotoxic T-Lymphocyte-Associated Protein 4 Blockade: Insights into Pathogenesis from an Autopsy Series. Am J Pathol. 2016; 186(12):3225–3235. https://doi.org/10.1016/j.ajpath.2016.08.020 PMID: 27750046

22. Joshi MN, Whitelaw BC, Palomar MT, Wu Y, Carroll PV. Immune checkpoint inhibitor-related hypophysitis and endocrine dysfunction: clinical review. Clin Endocrinol (Oxf). 2016; 85(3):331–339. https://doi.org/10.1111/cen.13063 PMID: 26998595

23. Joshi MN, Whitelaw BC, Carroll PV. MECHANISMS IN ENDOCRINOLOGY: Hypophysitis: diagnosis and treatment. Eur J Endocrinol. 2018; 179(3):R151–R163. https://doi.org/10.1530/EJE-17-0009 PMID: 29880706

24. Lin HH, Gutenberg A, Chen TY, Tsai NM, Lee CJ, Cheng YC, et al. In Situ Activation of Pituitary-Infiltrating T Lymphocytes in Autoimmune Hypophysitis. Sci Rep. 2017; 7(43492). https://doi.org/10.1038/srep43492 PMID: 28262761

25. Mortensen MJ, Oatman O, Azadi A, Fonkem E, Yuen KCJ. An Update on Immune Checkpoint Inhibitor-related Hypophysitis. US Endocrinol. 2020; 16(2):117–124. https://doi.org/10.17925/USE.2020.16.2.117

26. König D, Läubli H. Mechanisms of Immune-Related Complications in Cancer Patients Treated with Immune Checkpoint Inhibitors. Pharmacology. 2021; 106(3-4):123–136. https://doi.org/10.1159/000509081 PMID: 32721966

27. Faje A, Reynolds K, Zubiri L, Lawrence D, Cohen JV, Sullivan RJ, et al. Hypophysitis secondary to nivolumab and pembrolizumab is a clinical entity distinct from ipilimumab-associated hypophysitis. Eur J Endocrinol. 2019; 181(3):211–219. https://doi.org/10.1530/EJE-19-0238 PMID: 31176301

28. Franzen D, Schad K, Kowalski B, Clarenbach CF, Stupp R, Dummer R, et al. Ipilimumab and early signs of pulmonary toxicity in patients with metastastic melanoma: a prospective observational study. Cancer Immunol Immunother. 2018; 67(1):127–134. https://doi.org/10.1007/s00262-017-2071-2 PMID: 28983773

29. Zhu S, Fu Y, Zhu B, Zhang B, Wang J. Pneumonitis Induced by Immune Checkpoint Inhibitors: From Clinical Data to Translational Investigation. Front Oncol. 2020; 10 (1785). https://doi.org/10.3389/fonc.2020.01785 PMID: 33042827

30. Makunts T, Saunders IM, Cohen IV, Li M, Moumedjian T, Issa MA, et al. Myocarditis occurrence with cancer immunotherapy across indications in clinical trial and post-marketing data. Sci Rep. 2021; 11(17324). https://doi.org/10.1038/s41598-021-96467-5 PMID: 34462476

31. Samson K. In the Clinic Risks Reported for Neurologic Adverse Events with Two Cancer Immunotherapies. NeurologyToday. 2017; 17(20):1–22.

32. Bellaguarda E, Hanauer S. Checkpoint inhibitor-induced colitis. Am J Gastroenterol. 2020; 115(2):202–210. https://doi.org/10.14309/ajg.0000000000000497 PMID: 31922959

33. Seethapathy H, Zhao S, Chute DF, Zubiri L, Oppong Y, Strohbehn I, et al. The Incidence, Causes, and Risk Factors of Acute Kidney Injury in Patients Receiving Immune Checkpoint Inhibitors. Clin J Am Nephrol. 2019; 14(12):1692–1700. https://doi.org/10.2215/CJN.00990119 PMID: 31672794

34. Rogers BB, Cuddahy T, Zawislak C. Management of Acute Pancreatitis Associated With Checkpoint Inhibitors. J Adv Pract Oncol. 2020; 11(1):49–62. https://doi.org/10.6004/jadpro.2020.11.1.3 PMID: 33542849

35. De Martin E, Michot JM, Rosmorduc O, Guettier C, Samuel D. Liver toxicity as a limiting factor to the increasing use of immune checkpoint inhibitors. JHEP Rep. 2020; 2(6).

36. Gresnigt MS, van de Veerdonk FL. Chapter 8—Modulating Inflammatory Cytokines: IL-1. Immune Rebalancing, The Future of Immunosuppression. 2016; p. 151–171. https://doi.org/10.1016/B978-0-12-803302-9.00008-7

37. O'Brien SA, Zhu M, Zhang W. The Importance of IL-6 in the Development of LAT-Mediated Autoimmunity. J Immunol. 2015; 195(2):695–705. https://doi.org/10.4049/jimmunol.1403187 PMID: 26034173

38. Mehta AK, Gracias DT, Croft M. TNF activity and T cells. Cytokine. 2018; 101:14–18. https://doi.org/10.1016/j.cyto.2016.08.003 PMID: 27531077

39. Lai X, Friedman A. Combination therapy of cancer with cancer vaccine and immune checkpoint inhibitors: A mathematical model. PLoS ONE. 2017; 12(5):1–24. https://doi.org/10.1371/journal.pone.0178479 PMID: 28542574

40. Lai X, Friedman A. Combination therapy for melanoma with BRAF/MEK inhibitor and immune checkpoint inhibitor: a mathematical model. BMC Systems Biology. 2017; 11(1):1–18. https://doi.org/10.1186/s12918-017-0446-9 PMID: 28724377

41. Lai X, Stiff A, Duggan M, Wesolowski R, Carson WE III, Friedman A. Modeling combination therapy for breast cancer with BET and immune checkpoint inhibitors. PNAS. 2018; 115(21):5534–5539. https://doi.org/10.1073/pnas.1721559115 PMID: 29735668

42. Friedman A, Lai X. Combination therapy for cancer with oncolytic virus and checkpoint inhibitor: A mathematical model. PLoS ONE. 2018; 13(2):1–21. https://doi.org/10.1371/journal.pone.0192449 PMID: 29420595

43. Lai X, Friedman A. How to schedule VEGF and PD-1 inhibitors in combination cancer therapy? BMC Syst Biol. 2019; 13(30):1–18. https://doi.org/10.1186/s12918-019-0706-y PMID: 30894166

44. Siewe N, Friedman A. Combination therapy for mCRPC with immune checkpoint inhibitors, ADT and vaccine: A mathematical model. PLoS ONE. 2022; 17(1):e0262453. https://doi.org/10.1371/journal.pone.0262453 PMID: 35015785

45. Lai X, Hao W, Friedman A. TNF-α inhibitor reduces drug-resistance to anti-PD-1: A mathematical model. PLoS ONE. 2020; 15(4):1–21. https://doi.org/10.1371/journal.pone.0231499 PMID: 32310956

46. Siewe N, Friedman A. TGF-β inhibition can overcome cancer primary resistance to PD-1 blockade: a mathematical model. PLoS ONE. 2021; 16(6):1–16. https://doi.org/10.1371/journal.pone.0252620 PMID: 34061898

47. Nikolopoulou E, Eikenberry SE, Gevertz JL, Kuang Y. Mathematical modeling of an immune checkpoint inhibitor and its synergy with an immunostimulant. DCDS-B. 2021; 26(4):2133–2159. https://doi.org/10.3934/dcdsb.2020138

48. Radunskaya A, Kim R, Woods T II. Mathematical Modeling of Tumor Immune Interactions: A Closer Look at the Role of a PD-L1 Inhibitor in Cancer Immunotherapy. Spora: A Journal of Biomathematics. 2018; 4:25–41.

49. Lai X, Friedman A. Mathematical modeling of cancer treatment with radiation and PD-L1 inhibitor. Sci China Math. 2020; 63:465–484. https://doi.org/10.1007/s11425-019-1648-6

50. Serre R, Benzekry S, Padovani L, Meille C, André N, Ciccolini J, et al. Mathematical Modeling of Cancer Immunotherapy and Its Synergy with Radiotherapy. Cancer Res. 2016; 76(17):4931–4940. https://doi.org/10.1158/0008-5472.CAN-15-3567 PMID: 27302167

51. Yamane H, Igarashi O, Kato T, Nariuchi H. Positive and negative regulation of IL-12 receptor expression of naive CD4+T cells by CD28/CD152 co-stimulation. Eur J Immunol. 2000; 30:3171–3180. https://doi.org/10.1002/1521-4141(200011)30:11%3C3171::AID-IMMU3171%3E3.0.CO;2-C PMID: 11093132

52. Nelson BH. IL-2, regulatory T cells, and tolerance. J Immunol. 2004; 172(7):3983–3988. https://doi.org/10.4049/jimmunol.172.7.3983 PMID: 15034008

53. Ross SH, Cantrell DA. Signaling and Function of Interleukin-2 in T Lymphocytes. Annu Rev Immunol. 2018; 36:411–433. https://doi.org/10.1146/annurev-immunol-042617-053352 PMID: 29677473

54. Perrot CY, Javelaud D, Mauviel A. Insights into the transforming growth factor-beta signaling pathway in cutaneous melanoma. Ann Dermatol. 2013; 25(2):135–144. https://doi.org/10.5021/ad.2013.25.2.135 PMID: 23717002

55. Whiteside TL. The role of regulatory t cells in cancer immunology. Immunotargets Ther. 2015; 4:159–171. https://doi.org/10.2147/ITT.S55415 PMID: 27471721

56. Tran DQ. TGF-β: the sword, the wand, and the shield of FOXP3(+) regulatory T cells. J Mol Cell Biol. 2012; 4(1):29–37. https://doi.org/10.1093/jmcb/mjr033 PMID: 22158907

57. McNally A, Hill GR, Sparwasser T, Thomas R, Steptoe RJ. CD4+CD25+ regulatory T cells control CD8+ T-cell effector differentiation by modulating IL-2 homeostasis. Proc Natl Acad Sci U S A. 2011; 108(18):7529–34. https://doi.org/10.1073/pnas.1103782108 PMID: 21502514

58. Sims GP, Rowe DC, Rietdijk ST, Herbst R, Coyle AJ. Hmgb1 and rage in inflammation and cancer. Annu Rev Immunol. 2010; 28:367–388. https://doi.org/10.1146/annurev.immunol.021908.132603 PMID: 20192808

59. Palucka J, Banchereau J. Cancer immunotherapy via dendritic cells. Nat Rev Cancer. 2012; 12(4):265–277. https://doi.org/10.1038/nrc3258 PMID: 22437871

60. Saenz R, Futalan D, Leutenez L, Eekhout F, Fecteau JF, Sundelius S, et al. Tlr4-dependent activation of dendritic cells by an hmgb1-derived peptide adjuvant. J Transl Med. 2014; 12(211):1–11. https://doi.org/10.1186/1479-5876-12-211 PMID: 25123824

61. Ma Y, Shurin GV, Peiyuan Z, Shurin MR. Dendritic cells in the cancer microenvironment. J Cancer. 2013; 4(1):36–44. https://doi.org/10.7150/jca.5046 PMID: 23386903

62. Janco JMT, Lamichhane P, Karyampudi L, Knutson KL. Tumor-infiltrating dendritic cells in cancer pathogenesis. J Immunol. 2015; 194(7):2985–2991. https://doi.org/10.4049/jimmunol.1403134

63. Krishnan T, Tomita Y, Roberts-Thomson R. A retrospective analysis of eosinophilia as a predictive marker of response and toxicity to cancer immunotherapy. Future Sci OA. 2020; 6(10):FSO608. https://doi.org/10.2144/fsoa-2020-0070 PMID: 33312694

64. RELX Group (TM). Interleukin 12: Interleukin-12 (IL-12) is a potent proinflammatory cytokine that enhances the cytotoxic activity of T lymphocytes and resting natural killer cells. Pediatric Surgery, Seventh Ed. 2012;217.

65. Ha D, Tanaka A, Kibayashi T, Tanemura A, Sugiyama D, Wing JB, et al. Differential control of human Treg and effector T cells in tumor immunity by Fc-engineered anti–CTLA-4 antibody. PNAS. 2019; 116(2):609–618. https://doi.org/10.1073/pnas.1812186116 PMID: 30587582

66. Du X, Tang F, Liu M, Su J, Zhang Y, Wu W, et al. A reappraisal of CTLA-4 checkpoint blockade in cancer immunotherapy. Cell Res. 2018; 28:416–432. https://doi.org/10.1038/s41422-018-0011-0 PMID: 29472691

67. Rudd CE. CTLA-4 co-receptor impacts on the function of Treg and CD8+ T-cell subsets. Eur J Immunol. 2012; 39(3):687–690. https://doi.org/10.1002/eji.200939261

68. Maute RL, Gordon SR, Mayer AT, McCracken MN, Natarajan A, Ring NG, et al. Engineering high-affinity PD-1 variants for optimized immunotherapy and immuno-PET imaging. Proc Natl Acad Sci USA. 2015; 112(47):E6506–14. https://doi.org/10.1073/pnas.1519623112 PMID: 26604307

69. Cheng X, Veverka V, Radhakrishnan A, Waters LC, Muskett FW, Morgan SH, et al. Structure and interactions of the human programmed cell death 1 receptor. J Biol Chem. 2013; 288(17):11771–11785. https://doi.org/10.1074/jbc.M112.448126 PMID: 23417675

70. Tokunaga A, Sugiyama D, Maeda Y, Warner AB, Panageas KS, Ito S, et al. Selective inhibition of low-affinity memory CD8+ T cells by corticosteroids. J Exp Med. 2019; 216(12):2701–2713. https://doi.org/10.1084/jem.20190738 PMID: 31537643

71. Momtaz P, Park V, Panageas KS, Postow MA, Callahan M, Wolchok JD, et al. Safety of Infusing Ipilimumab Over 30 Minutes. J Clin Oncol. 2015; 33(30):3454–3458. https://doi.org/10.1200/JCO.2015.61.0030 PMID: 26124475

72. RxList. YERVOY, Generic Name: ipilimumab injection. Accessed March 12, 2021; p. https://www.rxlist.com/yervoy–drug.htm.

73. Drugs com. How long does it take prednisone to get out of your system? https://www.drugs.com/medical-answers/prednisone-how-long-does-it-take-predesone-to-get-372449/. Last updated on March 22, 2021.

74. Aldea M, Orillard E, Mansi L, Marabelle A, Scotte F, Lambotte O, et al. How to manage patients with corticosteroids in oncology in the era of immunotherapy? Eur J Cancer. 2020; 141:239–251. https://doi.org/10.1016/j.ejca.2020.09.032 PMID: 33212339

75. Linxweiler J, Körbel C, Müller A, Hammer M, Veith C, Bohle RM, et al. A novel mouse model of human prostate cancer to study intraprostatic tumor growth and the development of lymph node metastases. Prostate. 2018; 78(9):664–675. https://doi.org/10.1002/pros.23508 PMID: 29572953

76. Lemech C, Arkenau HT. Novel treatments for metastatic cutaneous melanoma and the management of emergent toxicities. Clin Med Insights Oncol. 2012; 6:53–66. https://doi.org/10.4137/CMO.S5855 PMID: 22253555

77. Diao J, Winter E, Cantin C, Chen W, Xu L, Kelvin D, et al. In Situ Replication of Immediate Dendritic Cell (DC) Precursors Contributes to Conventional DC Homeostasis in Lymphoid Tissue. J Immunol. 2006; 176(12):7196–7206. https://doi.org/10.4049/jimmunol.176.12.7196 PMID: 16751363

78. Rocha B, Freitas AA, Coutinho AA. Population dynamics of T lymphocytes. Renewal rate and expansion in the peripheral lymphoid organs. J Immunol. 1983; 131(5):2158–2164. PMID: 6605376

79. Furlan SN, Singh K, Lopez C, Tkachev V, Hunt DJ, Hibbard J, et al. IL-2 enhances ex vivo–expanded regulatory T-cell persistence after adoptive transfer. Blood Adv. 2020; 4(8):1594–1605. https://doi.org/10.1182/bloodadvances.2019001248 PMID: 32311015

80. Lotze MT, Frana LW, Sharrow SO, Robb RJ, Rosenberg SA. In vivo administration of purified human interleukin 2. I. Half-life and immunologic effects of the Jurkat cell line-derived interleukin 2. J Immunol. 1985; 134(1):157–166. PMID: 3871099

81. Jung K, Ha J, Kim J, Kim J, Kim Y, Kim C, et al. Heterodimeric Fc-fused IL12 shows potent antitumor activity by generating memory CD8+ T cells. OncoImmunol. 2018; 7(7). https://doi.org/10.1080/2162402X.2018.1438800 PMID: 29900039

82. Friedman A, Siewe N. Chronic Hepatitis B Virus and Liver Fibrosis: A Mathematical Model. PLoS ONE. 2018; 13(4):1–23. https://doi.org/10.1371/journal.pone.0195037 PMID: 29634771

83. Simo R, Barbosa-Desongles A, Lecube A, Hernandez C, Selva DM. Potential Role of Tumor Necrosis Factor-α in Downregulating Sex Hormone–Binding Globulin. Diabetes. 2012; 61:372–382. https://doi.org/10.2337/db11-0727 PMID: 22210320

84. Fellner C. Ipilimumab (yervoy) prolongs survival in advanced melanoma: serious side effects and a hefty price tag may limit its use. P & T. 2012; 37(9):503–530.

85. Drugs com. Medrol Dosepak—How long does a dose pack stay in your system? 2020.

86. Hornbeck PV, Zhang B, Murray B, Kornhauser JM, Latham V, Skrzypek E. PhosphoSitePlus, 2014: mutations, PTMs and recalibrations. Nucleic Acids Research. 2015; 43:D512–D520. https://doi.org/10.1093/nar/gku1267 PMID: 25514926

87. Young ME. Estimation of diffusion coefficients of proteins. Biotech Bioeng. 1980; XXII:947–955. https://doi.org/10.1002/bit.260220504

88. Michalaki V, Syrigos K, Charles P, Waxman J. Serum levels of IL-6 and TNF-α correlate with clinico-pathological features and patient survival in patients with prostate cancer. Br J Cancer. 2004; 90:2312–2316. https://doi.org/10.1038/sj.bjc.6601814 PMID: 15150588

89. National Center for Biotechnology Information. PubChem Compound Summary for CID 56842206, TGF-beta. PubChem, https://pubchem.ncbi.nlm.nih.gov/compound/TGF-beta. Accessed January 24, 2021.

90. Abcam. Recombinant Anti-CTLA4 antibody [EPR1476] (ab134090). https://www.abcam.com/ctla4-antibody-epr1476-ab134090html.

91. National Center for Biotechnology Information. PubChem Compound Summary for CID 5755, Predniso-lone. https://pubchem.ncbi.nlm.nih.gov/compound/Prednisolone. Accessed September 29, 2021.

92. Eckert F, Schaedle P, Zips D, Schmid-Horche B, Rammensee H, Gani C, et al. Impact of curative radio-therapy on the immune status of patients with localized prostate cancer. Oncoimmunol. 2018; 7(11): e1496881 (11 pages). https://doi.org/10.1080/2162402X.2018.1496881 PMID: 30393582

93. Tazaki E, Shimizu N, Tanaka R, Toshizumi M, Kamma H, Imoto S, et al. Serum cytokine profiles in patients with prostate carcinoma. Exp Ther Med. 2011; 2(5):887–891. https://doi.org/10.3892/etm.2011.286 PMID: 22977593